

---

# Differentiable Invariant Causal Discovery

---

Yu Wang<sup>1</sup>, An Zhang<sup>2,3\*</sup>, Xiang Wang<sup>4</sup>, Xiangnan He<sup>4</sup>, Tat-Seng Chua<sup>2,3</sup>

<sup>1</sup>University of California, San Diego,

<sup>2</sup>Sea-NExT Joint Lab, <sup>3</sup>National University of Singapore,

<sup>4</sup>University of Science and Technology of China

yuw164@ucsd.edu, {an\_zhang, dcscts}@nus.edu.sg

{xiangwang1223, xiangnanhe}@gmail.com,

## Abstract

Learning causal structure from observational data is a fundamental challenge in machine learning. However, the majority of commonly used differentiable causal discovery methods are non-identifiable, turning this problem into a continuous optimization task prone to data biases. In many real-life situations, data is collected from different environments, in which the functional relations remain consistent across environments, while the distribution of additive noises may vary. This paper proposes Differentiable Invariant Causal Discovery (DICD), utilizing the multi-environment information based on a differentiable framework to avoid learning spurious edges and wrong causal directions. Specifically, DICD aims to discover the environment-invariant causation while removing the environment-dependent correlation. We further formulate the constraint that enforces the target structure equation model to maintain optimal across the environments. Theoretical guarantees for the identifiability of proposed DICD are provided under mild conditions with enough environments. Extensive experiments on synthetic and real-world datasets verify that DICD outperforms state-of-the-art causal discovery methods up to 36% in SHD. Our code will be open-sourced upon acceptance.

## 1 Introduction

Causal discovery (CD) is a fundamental problem in a variety of tasks, such as understanding the generation process of data [51], and probing explainability of models [36, 46]. It has tremendous impacts on various domains like biology [32, 28] and finance [34]. CD aims to learn the causal structure among a set of variables from the observational data and present the structure as a directed acyclic graph (DAG). The acyclicity constraint frames CD as the combinatorial optimization of discrete edges, which however, is NP-hard. Recently, leading CD solutions [51, 47, 53, 21] gracefully convert the DAG learning into the continuous optimization task. Specifically, the idea stemming from NOTEARS [51] is to build a scoring function upon the adjacency matrix over the variables and find an equivalent continuous constraint on acyclicity.

NOTEARS [51] inspired the development of numerous differentiable causal discovery algorithms that use gradient descent to find the optimal causal graph [52, 3, 48]. When compared to traditional constraint-based causal discovery, these methods have demonstrated superior performance and efficiency in uncovering the true graph with a large amount of data. However, most of them follow the paradigm of empirical risk minimization (ERM) [44] — first imposing the scored DAG on the observations to reconstruct, and then minimizing the empirical risks between the observational and reconstructed data, so as to optimize the DAG. Despite the promising performance, we argue that ERM is prone to capture data biases or shortcut [1, 33, 4], thus derailing the structure learning of DAG. Specifically, the observations of variables are often marred by some spurious correlations, such as the annotator or selection biases in the data acquisition pipeline [1], thus posing undesired

---

\* An Zhang is the corresponding author.

Table 1: Examples that NOTEARS would find the wrong causal graph while multi-environment settings can help identify the true graph. We present the DAGs derived from minimal reconstruction loss in different environments. The graph on the left denotes the ground truth. The edges in red are wrong or spurious, while the dash one represents the corresponding coefficient is zero. We list the reconstruction loss value following with the triplets in brackets representing coefficients of  $Y$  with  $A, B$  and  $C$ . The loss values and parameters of the potential sub-optimal causal structures learned by NOTEARS in a single environment are highlighted in red. Detailed data generating processes are as follows.  $X \sim \mathcal{N}(0, 1)$ ,  $A = X + z_A (\sim \mathcal{N}(0, 1))$ ,  $B = X + Y/2 + z_B^e (\sim \mathcal{N}(0, (\sigma_B^e)^2))$ ,  $C = X/2 + z_C^e (\sim \mathcal{N}(0, (\sigma_C^e)^2))$ ,  $Y = A/4 + \epsilon_Y (\sim \mathcal{N}(0, 1))$ .  $\sigma_B^e$  and  $\sigma_C^e$  varies across three environments,  $e_1, e_2$  and  $e_3$ , with  $(\sigma_B^e)^2 = (\sigma_C^e)^2 = 1, 2, 4$ , respectively.

		Ground Truth DAG		
		$X \rightarrow A$	$X \rightarrow B$	$X \rightarrow C$
$e_1$		4.57(0.24, 1.14, -1.32)	5.07(0.24, 0.32, 0.00)	5.07(0.24, 0.50, 0.00)
$e_2$		6.59(0.24, 1.09, -1.19)	7.14(0.24, 0.23, 0.00)	7.07(0.24, 0.50, 0.00)
$e_3$		10.60(0.24, 1.07, -1.12)	11.21(0.24, 0.15, 0.00)	11.07(0.24, 0.50, 0.00)
5.00(0.25, 0.50, 0.00)	$e_1$	5.05(0.24, 0.50, 0.10)	4.57(-0.23, 1.38, -1.54)	5.12(0.07, 0.29, 0.00)
7.00(0.25, 0.50, 0.00)	$e_2$	7.06(0.24, 0.50, 0.06)	6.59(-0.24, 1.36, -1.44)	7.17(0.14, 0.18, 0.00)
11.00(0.25, 0.50, 0.00)	$e_3$	11.06(0.24, 0.50, 0.03)	10.59(-0.24, 1.35, -1.39)	11.21(0.18, 0.11, 0.00)

entanglements of variables. ERM easily latches on these correlations [1, 20, 33] to refine the DAG structure, as the following example illustrates.

Consider the ground-truth DAG in Table 1 as the target being reconstructed by the CD solutions, where each edge denotes a causal relationship between two variable nodes.  $X$  consists of three variables, which have different relationships with  $Y$ :  $A$  determines  $Y$ ,  $B$  is influenced by  $Y$ , and  $C$  is irrelevant to  $Y$ . While the CD solutions are designed to identify the causation edges, ERM does not need to learn the correct DAG to reach a low reconstruct loss for fitting the observations. For example, instead of looking at the true causation  $B \leftarrow Y$ , it is easy to capture the statistical shortcut edge  $B \rightarrow Y$ , since  $B$  is strongly correlated with  $Y$  and the reconstructed DAGs achieve even lower losses as compared to the ground-truth DAG. This common problem is consistent with over-reconstruction [13] but remains largely unexplored.

In this study, we aim to design a paradigm that distinguishes the causation edges from spuriously-correlated edges and obtains the faithful DAG. Although learning causal structure from observational data is challenging, we draw inspiration from invariant learning [1, 20, 33] and approximate the task by searching the edges with *invariant* structural equations in multi-environment settings. Across different environments, only factual causation edges remain invariant, while spurious edges or edges with wrong causal directions hardly remain stable, according to the assumptions in *invariant learning* [1]. Though reminiscent of past ideas - *e.g.*, causal structure learning in multi-domain, from heterogeneous/nonstationary data [30, 11, 16, 12, 15, 5, 31] - these methods are only applicable in a linear system or restricted to conditional independence tests, which suffer from high computation complexity as the number of variables increases. To achieve effective differentiable causal discovery in both linear and nonlinear scenarios, we reconsider Table 1 and additionally exhibit the multi-environment information, which impacts the distributions of additive noises. Applying ERM on these environments separately results in different functions when there exist spurious correlations in the causal graph. This inspires us to exclude such unstable edges towards a robust DAG across environments.

Towards this end, we propose **differentiable invariant causal discovery** (DICD), a novel scheme of DAG structure learning that incorporates the idea of invariant learning — that is, learning an invariant DAG with the piece of environment information. Specifically, a DAG generator module learns to generate the environment-aware DAGs from individual environments. For each DAG, the structure equation model (SEM) [29] describes the functions of learned causation edges. We then exploit the principle of invariant risk minimization (IRM) [1] to encourage the SEMs to be optimal

across all environments, so as to obtain DAGs regardless of environment changes. On synthetic and real-world datasets, extensive experiments demonstrate the effectiveness of DICD to surpass current state-of-the-art CD solutions.

Our main contributions are:

- To the best of our knowledge, we are among the first class to adopt the environment information into the differentiable causal discovery framework.
- We propose a novel causal discovery solution, DICD, to incorporate the invariant learning on both linear and nonlinear settings. Experimental results on synthetic and real-world datasets demonstrate that DICD could significantly better reveal true correlations and eliminate the spurious ones compared with prevalent methods.
- We provide theoretical guarantees for the identifiability of proposed DICD in linear systems under mild conditions, given certain assumptions about the environments.

## 2 Preliminary

We begin with the assumptions as the basis of our work, then give the task formulation of causal discovery (CD). After that, we introduce the continuous optimization paradigm via empirical risk minimization (ERM), as well as the linear and nonlinear solutions. We list notations in Appendix A.

**Assumptions.** (i) The structural equations are invariant across different environments; (ii) The system is causally sufficient; (iii) Observational data is generated from a structural equation model with independent additive noise.

The assumption (i) - (iii) are crucial to our method and provide the key insight into how causal structure can be identified from observational data. Assumption (i) states that the invariance principle is held across environments. Assumption (ii) ensures that no hidden confounders exist in the system. In other words, there is no systematic bias induced by hidden confounders.

**Task Formulation of CD.** Let  $\mathbf{X} = [\mathbf{x}_1 | \dots | \mathbf{x}_d] \in \mathbb{R}^{n \times d}$  denote the  $n$  observational data of  $d$  variables, which are generated from a target directed acyclic graph (DAG). The target DAG is  $(\mathcal{V}, \mathcal{D})$ , where  $\mathcal{V}$  represents the set of node variables, denoted as  $\{X_1, \dots, X_d\}$ . And  $\mathcal{D}$  is the set of cause-effect edges between variables. The observational data is assumed to be generated from the following SEM:

$$X_j = F_j(Pa(X_j)) + z_j, j \in \{1, \dots, d\} \quad (1)$$

where  $X_j$  is the  $j$ -th node variable,  $F_j$  is the causal structure function,  $Pa(X_j)$  is the set of the parents of  $X_j$ , and  $z_j$  refers to the additive noise with variance  $\sigma_j^2$ . Without loss of generality, we assume that the noises are zero-mean. In real-life settings, since the dataset may be obtained from various environments, the distribution of additive noises  $z_j$  may differ across different environments. The causal structure function  $F_j$ , on the other hand, generally remains constant. The goal of CD is to learn a DAG to reconstruct the observations  $\mathbf{X}$ . The acyclicity restriction of DAG is the fundamental obstacle, because it frames DAG learning as a NP-hard combinatorial optimization task.

**Common Paradigm of ERM.** Leading differentiable CD solutions, *e.g.*, NOTEARS [51] and its follow-on studies [52, 48], convert DAG learning into a continuous optimization process to overcome this obstacle. The primary idea is to build a scoring function upon the adjacency matrix of variables and discover an equivalent continuous constraint on acyclicity. To optimize the scoring function, they mostly adopt the paradigm of ERM to minimize the empirical risks between the observational and reconstructed data as follows:

$$\min_f \mathcal{L}(f) = \frac{1}{N} \sum_{i=1}^d l(\mathbf{x}_i, f_i(\mathbf{X})), \quad \text{s.t. } \mathcal{G}(f) \in \text{DAG}, \quad (2)$$

where  $\mathbf{x}_i$  is the observations of node variable  $X_i$ , and  $l(\cdot, \cdot)$  is the reconstruction loss function, *i.e.*, squared loss or negative log-likelihood.  $f = (f_1, \dots, f_d)$  formulates the estimated structure function [29] of variables, where  $f_i : \mathbb{R}^{n \times d} \rightarrow \mathbb{R}^n$  is the estimated structure function of node variable  $X_i$ .  $f_i(X_1, \dots, X_d)$  is dependent on  $X_j$ , if  $X_j \in Pa(X_i)$ . The score-based solutions seek to learn  $f$  conditioning on the DAG constraint:  $\mathcal{G}(f) \in \text{DAG}$ .

Following prior studies [51, 52], we use the adjacency matrix  $\mathbf{W} \in \mathbb{R}^{d \times d}$  to encode the graph  $\mathcal{G}(f)$ , where each element  $[\mathbf{W}]_{ij} \neq 0$  indicates the existence of edge  $X_i \rightarrow X_j$ . The previous work [52]

defines the non-parametric acyclicity upon the entries of matrix  $\mathbf{W}(f) = \mathbf{W}(f_1, \dots, f_d)$  as follows:

$$[\mathbf{W}(f)]_{ij} := \|\partial_i f_j\|_2 > 0, \quad (3)$$

where  $\partial_i f_j$  is  $f_j$ ’s partial derivation w.r.t.  $X_i$ ; as such,  $f_j$  does not depend on  $X_i$  if and only if  $\|\partial_i f_j\|_2 = 0$ , where  $\|\cdot\|_2$  is the  $L^2$  or Frobenius norm. With Eq.(3), we can exploit linear and nonlinear functions  $f$  to characterize acyclicity in linear and nonlinear SEMs, respectively.

**Linear SEM.** In the case of linear SEM [51], we formulate  $f(\mathbf{X})$  as a linear matrix multiplication:  $f(\mathbf{X}) = \mathbf{XA}$ , where  $\mathbf{A} \in \mathbb{R}^{d \times d}$  denotes the coefficient matrix. This formulation frames the acyclicity in Eq.(3) as:

$$[\mathbf{W}(f)]_{ij} = \|A_{ij}\|_2. \quad (4)$$

**Nonlinear SEM.** In the case of nonlinear SEM [52], we define  $f_i(\mathbf{X})$  as a multilayer perceptron (MLP) with  $h$  hidden layers and an activation function  $\sigma$  as:

$$f_i(\mathbf{X}) = \text{MLP}(\mathbf{X}; \mathbf{A}_i^{(1)}, \dots, \mathbf{A}_i^{(h)}) = \sigma(\dots \sigma(\mathbf{X}\mathbf{A}_i^{(1)}) \dots) \mathbf{A}_i^{(h)}, \quad (5)$$

where  $\mathbf{A}_i^{(l)} \in \mathbb{R}^{m_{l-1} \times m_l}$  is the learnable matrix of the  $l$ -th hidden layer for the  $i$ -th node; and  $m_l$  is the number of hidden units in the  $l$ -th layer,  $m_0 = d$ . According to [52], this formulation frames the acyclicity in Eq.(3) as:

$$[\mathbf{W}(f)]_{ij} = \left\| \text{i-th column}(\mathbf{A}_j^{(1)}) \right\|_2. \quad (6)$$

### 3 Methodology

In this section, we first present differentiable invariant causal discovery (DICD) to conduct causal structural learning over multiple environments. We then detail the formulations in both linear and nonlinear settings.

#### 3.1 Differentiable Invariant Causal Discovery (DICD)

Despite the great success, the ERM paradigm easily captures spurious correlations between variables by over-reconstructing the observations [13] (See toy example in Table 1). It is important to distinguish the causation edges from the spuriously-correlated edges. Towards this end, we get access to the multi-environment information and incorporate the idea of invariant learning, so as to frame the causal discovery task as identifying environment-invariant causation edges and discarding environment-dependent correlations.

First, we argue that the multi-environment, in various forms like explicit or implicit metadata, is common in many real-world datasets and can partition the data into different groups or domains. The environments in LFW [18], for instance, can divide the data into black-and-white and colorful photographs. In ImageNet [6], the data can be grouped by different sources and years of images. Moreover, several benchmarks for the domain-shifts problems have been provided by WILDS [19]. Among them, Camelyon17 [2] includes the images collected from five hospitals that serve as different environments, while Amazon [26] provides review texts from different reviewers that can work as environments. Towards the end, the formal definition of the different environments in our paper is given as follow:

**Definition 3.1.** For two datasets generated from the same structure equation model as shown in Eq.(1). if there exists  $i \in \{1, \dots, d\}$  such that the distribution of  $z_i$  is different across these datasets and  $X_i$  is not the source node (see Definition C.1) in the corresponding graph. Then we say these two datasets are drawn from different environments.

With the environment information, we utilize the invariant learning to conduct multi-environment causal discovery — the function parameters of SEM from the target DAG should remain optimal across all the environments. Guided by this idea, DICD consists of two modules: (1) Invariant structural model  $\mathbf{S}$ , which presents the structure of DAG, *i.e.*, a binary adjacency matrix. By “invariant”, we mean that  $\mathbf{S}$  should be consistent across environments; and (2) Optimal causal function  $f$ , which depicts the causal relation of variables. By “optimal”, we mean that  $f$  should be optimal over all the environments once the structural model  $\mathbf{S}$  is given. Considering Table 1 again,  $\mathbf{S}$  is the DAG structure, while  $f$  refers to the coefficients of edges. On the basis of  $\mathbf{S}$  and  $f$  across environments, we may exclude the wrong DAGs with lower reconstruction losses than the ground-truth DAG.

Having the environment-aware groups of observations, we can define the empirical risk within the environment  $e \in \mathcal{E}$  as:

$$\mathcal{L}^e(\mathbf{S} \circ f) = \frac{1}{n_e} \sum_{i=1}^d l(\mathbf{X}_i^e, (\mathbf{S} \circ f)_i(\mathbf{X}^e)), \quad (7)$$

where  $(\mathbf{S} \circ f)_i(\mathbf{X}^e)$  is the vector of the  $i$ -th column of the reconstructed matrix  $(\mathbf{S} \circ f)(\mathbf{X}^e)$ . Upon the losses of individual environments, we build two constraints on  $\mathbf{S}$  and  $f$  across all environments, and establish the objective function of DICD:

$$\min_{\mathbf{S} \circ f} \sum_{e \in \mathcal{E}} \mathcal{L}^e(\mathbf{S} \circ f), \quad (8)$$

$$\text{s.t. } \mathcal{G}(\mathbf{S}) = \mathcal{G}(f) \in \text{DAG}, \quad (9)$$

$$f = \arg \min_{\bar{f}} \mathcal{L}^e(\mathbf{S} \circ \bar{f}), \quad \forall e \in \mathcal{E}. \quad (10)$$

Eq.(9) states that the DAGs represented by  $\mathbf{S}$  and  $f$  are equivalent, expressing that  $f$  latches on  $\mathbf{S}$ 's structure. Eq.(10) claims that  $f$  refers to the optimal causal model fitting Eq.(8). Following [52], we can rewrite Eq.(9) as:

$$\mathcal{G}(\mathbf{S}) = \mathcal{G}(f), \quad h(\mathbf{W}(f)) = 0, \quad (11)$$

where  $\mathbf{W}(f)$  is defined as Eq.(3), and  $h(\mathbf{W}) = \text{tr}(e^{\mathbf{W} \circ \mathbf{W}}) - d$ ,  $\circ$  is the Hadamard product, and  $e^{\mathbf{A}}$  is the matrix exponential of  $\mathbf{A}$ .

### 3.2 Linear SEM

When  $f$  characterizes acyclicity in the linear SEM, we have  $f(\mathbf{X}) = \mathbf{XA}$  and  $\partial_i f_j(\mathbf{X}) = A_{ij}$  (cf. Eq.(4)). With the invariant structure model  $\mathbf{S}$  as the binary matrix, we can convert  $\mathbf{S} \circ f$  as  $\mathbf{S} \circ \mathbf{A}$ , which is the Hadamard product (*aka.* the element-wise product) between  $\mathbf{S}$  and  $\mathbf{A}$ . We can simplify the learning of these two matrices as the optimization of a new matrix  $\mathbf{AS} = \mathbf{S} \circ \mathbf{A} \in \mathbb{R}^{d \times d}$ . As such, the loss function in Eq.(8) with the constraint in Eq.(9) is equivalent to:

$$\min_{\mathbf{AS}} \sum_{e \in \mathcal{E}} \mathcal{L}^e(\mathbf{AS}), \quad \text{s.t. } h(\mathbf{AS}) = 0. \quad (12)$$

Once  $\mathbf{AS}$  is learned, we can simply set  $\mathbf{A} = \mathbf{AS}$  and set  $\mathbf{S}$  as the binary indicator on  $\mathbf{AS}$ 's elements.

We then explore the tractable formulation for the constraint in Eq.(10) with the following theorem:

**Theorem 3.2.** *In the linear setting, we denote the parameters of the function  $f$  by  $\mathbf{A}$ . Given  $\mathbf{AS}$ , the optimality condition Eq.(10) is equivalent to*

$$\left\| \frac{\partial \mathcal{L}^e(\mathbf{AS} \circ \mathbf{A})}{\partial \mathbf{A}} \Big|_{\mathbf{A}=\mathbf{I}} \right\|_2^2 = 0, \quad \forall e \in \mathcal{E}, \quad (13)$$

where  $\mathbf{I}$  is the all-one matrix.

We give the detailed proof of the theorem in Appendix C.2. From Theorem 3.2, we could find that the intractable constraint Eq.(10) is now differentiable with the equivalent objective Eq.(13). With this theorem, we finally establish the objective function of DICD in linear cases as follows:

$$\min_{\mathbf{AS}} \sum_{e \in \mathcal{E}} \mathcal{L}^e(\mathbf{AS}) + \lambda \sum_{e \in \mathcal{E}} \left\| \frac{\partial \mathcal{L}^e(\mathbf{AS} \circ \mathbf{A})}{\partial \mathbf{A}} \Big|_{\mathbf{A}=\mathbf{I}} \right\|_2^2, \quad \text{s.t. } h(\mathbf{AS}) = 0. \quad (14)$$

This objective function potentially incorporates the invariant term and the coefficient into the single variable  $\mathbf{AS}$ , thus only adds one more penalty for training compared with NOTEARS.

### 3.3 Nonlinear SEM

For simplicity, we will continue to focus on the situation with scalar-valued variables (*i.e.*,  $\mathbf{X} \in \mathbb{R}^{n \times d}$ ). However, our method could be easily generalized into the vector-valued variables (*i.e.*,  $\mathbf{X} \in \mathbb{R}^{n \times d \times d_x}$ ). The extension from linear to nonlinear setting is based on [52]. We only need to apply the continuous DAG constraint on the matrix relevant to the first layer of all the MLPs. Also, we will apply the structure matrix  $\mathbf{S}$  on the first layer, *i.e.*, to ensure the parameters of MLP latch on the structure  $\mathbf{S}$ . In

this situation, with Eq.(5), we propose to simplify the learning of  $\mathbf{S}$  and  $f$  as the optimization of a new function  $f_{\mathbf{S}} = (f_{\mathbf{S}1}, \dots, f_{\mathbf{S}d})$ , where  $f_{\mathbf{S}i} = \mathbf{S} \circ f_i$ . The detailed formulation of  $f_{\mathbf{S}i}$  is:

$$f_{\mathbf{S}i} = \mathbf{S} \circ f_i = \text{MLP}(\text{Re}([\mathbf{S}]_i, m_1) \circ \mathbf{A}_i^{(1)}, \mathbf{A}_i^{(2)}, \dots, \mathbf{A}_i^{(h)}) = \text{MLP}(\mathbf{A}_{\mathbf{S}i}^{(1)}, \mathbf{A}_i^{(2)}, \dots, \mathbf{A}_i^{(h)}) \quad (15)$$

where  $m_1$  comes from  $\mathbf{A}_i^{(1)} \in \mathbb{R}^{m_0 \times m_1}$ , and  $\text{Re}([\mathbf{S}]_i, m_1)$  refers to  $\underbrace{[\mathbf{S}]_i, \dots, [\mathbf{S}]_i}_{m_1 \text{ times}}^\top$ , with  $[\mathbf{S}]_i$  being

the  $i$ -th column of  $\mathbf{S}$ . We denote  $\text{Re}([\mathbf{S}]_i, m_1) \circ \mathbf{A}_i^{(1)}$  as  $\mathbf{A}_{\mathbf{S}i}^{(1)}$ . Similar to the linear setting, once  $f_{\mathbf{S}}$  is learned, we can simply set  $f = f_{\mathbf{S}}$  and  $\mathbf{S}$  as the adjacency matrix of  $\mathcal{G}(f)$ . Then  $f$  and  $\mathbf{S}$  will share the same structure. Now we give the following theorem for nonlinear setting:

**Theorem 3.3.** *In nonlinear setting, we denote  $\mathbf{A}_i^{(l)}$ ,  $l \in \{1, \dots, d\}$  as the parameter of the  $l$ -th layer of MLP  $f_j$ , and  $\mathbf{A}_{\mathbf{S}j}$  is the parameter of the 1st layer of MLP  $f_j$ ,  $j \in \{1, \dots, d\}$ . Then given the matrix  $\mathbf{A}_{\mathbf{S}}$ , the optimal condition Eq.(10) is equivalent to*

$$\sum_{i=1}^d \left\| \frac{\partial \mathcal{L}^e(\text{MLP}(\mathbf{A}_{\mathbf{S}i} \circ \mathbf{A}_i^{(1)}, \mathbf{A}_i^{(2)}, \dots, \mathbf{A}_i^{(n)}))}{\partial \mathbf{A}_i^{(1)}} \Big|_{\mathbf{A}_i^{(1)} = \mathbf{I}} \right\|_2^2 = 0, \quad \forall e \in \mathcal{E}. \quad (16)$$

The detailed proof is given in Appendix C.3. With this theorem, we could transform the intractable constraint in Eq.(10) into the differentiable term subject to the first layer of MLP. The detailed formulation in the nonlinear setting can be expressed as:

$$\min_{f_{\mathbf{S}}} \sum_{e \in \mathcal{E}} L^e(f_{\mathbf{S}}) + \lambda \sum_{e \in \mathcal{E}} \sum_{i=1}^d \left\| \frac{\partial \mathcal{L}^e(\text{MLP}(\mathbf{A}_{\mathbf{S}i} \circ \mathbf{A}, \mathbf{A}_i^{(2)}, \dots, \mathbf{A}_i^{(n)}))}{\partial \mathbf{A}} \Big|_{\mathbf{A}=\mathbf{I}} \right\|_2^2, \quad \text{s.t. } h(\mathbf{W}(f_{\mathbf{S}})) = 0 \quad (17)$$

This objective function also potentially uses  $f_{\mathbf{S}}$  to both incorporate  $f$  and the invariant structure matrix  $\mathbf{S}$ . Compared to NOTEARS-MLP, only one regularization term is added.

## 4 Theoretical Analysis

In this section, we aim to provide the sufficient conditions for identifiability of DICD in the linear SEM systems. We will leave the discussion about which assumptions can or cannot be relaxed further in future work.

**Theorem 4.1.** *For linear SEMs systems with Gaussian additive noises as in Eq.(1), if for any  $X_i \in \mathcal{V}$  that is not the source node, there exist two environments  $e_1, e_2 \in \mathcal{E}$ , such that:*

$$\text{Var}(z_i^{e_1}) \neq \text{Var}(z_i^{e_2}) \quad (18)$$

$$\forall X_j \in \mathcal{V} \setminus \{X_i\}, \text{Var}(z_j^{e_1}) = \text{Var}(z_j^{e_2}) \quad (19)$$

where  $\text{Var}(\cdot)$  represents the variance,  $z_j^{e_1}$  and  $z_j^{e_2}$  are the additive noise from  $\text{Pa}(X_j)$  to  $X_j$  in  $e_1$  and  $e_2$ , respectively. Then the causal structure is **identifiable**.

Here we emphasize that the graph and the coefficients that satisfy the following sufficient conditions and Eq.(8-10) will be exactly the true causal graph and the true coefficients, corresponding to the identifiable graph. We provide the full proof of Theorem 4.1 in Appendix C.4. Theorem 4.1 indicates that our DICD is guaranteed to retrieve the true causal graph in linear systems, when the diversity of environments is adequate.

## 5 Experiments

In this section, we study the empirical performance of our proposed method given environments information from three aspects: 1) The overall performances of DICD compared to the previous methods in both linear and nonlinear settings. 2) The effects of various factors (*i.e.*, the number of environments, density of graph). 3) The performances of DICD and other applicable baselines on the real-world dataset.

### 5.1 Experimental Settings

We now provide the detailed settings for our experiments. The descriptions for the datasets are in Section 5.1.1. For all the experiments in this paper, we all generate 10 datasets for each graph setting and report the mean and standard deviation. We provide the descriptions of the baselines, hyperparameter settings, as well as evaluation protocols in Appendix D.2, D.3 and D.4, respectively.

Table 2: Linear Setting, for ER and SF graphs of 10, 20, 50 nodes

ER4	10 nodes			20 nodes			50 nodes		
	FDR	TPR	SHD	FDR	TPR	SHD	FDR	TPR	SHD
CD-NOD	0.48 $\pm$ 0.06	0.17 $\pm$ 0.02	33.5 $\pm$ 0.9	0.48 $\pm$ 0.19	0.11 $\pm$ 0.02	75.7 $\pm$ 5.0	0.56 $\pm$ 0.08	0.15 $\pm$ 0.06	195.0 $\pm$ 8.0
NOTEARS	0.07 $\pm$ 0.01	0.78 $\pm$ 0.02	10.1 $\pm$ 0.8	0.20 $\pm$ 0.03	0.71 $\pm$ 0.08	35.9 $\pm$ 7.4	0.27 $\pm$ 0.04	0.78 $\pm$ 0.03	96.7 $\pm$ 13.7
DAGGNN	0.08 $\pm$ 0.01	0.86 $\pm$ 0.02	7.6 $\pm$ 0.9	0.34 $\pm$ 0.04	0.79 $\pm$ 0.05	48.3 $\pm$ 7.1	0.36 $\pm$ 0.03	0.86 $\pm$ 0.03	122.3 $\pm$ 14.6
NoCurl	0.14 $\pm$ 0.01	0.81 $\pm$ 0.01	9.8 $\pm$ 0.4	0.19 $\pm$ 0.02	<b>0.92<math>\pm</math>0.01</b>	22.3 $\pm$ 2.4	0.31 $\pm$ 0.02	<b>0.94<math>\pm</math>0.01</b>	89.5 $\pm$ 9.5
DARING	0.08 $\pm$ 0.01	0.81 $\pm$ 0.03	9.3 $\pm$ 1.3	0.38 $\pm$ 0.07	0.58 $\pm$ 0.07	60.9 $\pm$ 9.9	0.48 $\pm$ 0.01	0.60 $\pm$ 0.06	187.6 $\pm$ 4.9
DICD	<b>0.03<math>\pm</math>0.01</b>	<b>0.88<math>\pm</math>0.02</b>	<b>4.9<math>\pm</math>1.0</b>	<b>0.16<math>\pm</math>0.03</b>	0.89 $\pm$ 0.04	<b>19.7<math>\pm</math>5.8</b>	<b>0.26<math>\pm</math>0.02</b>	0.89 $\pm$ 0.06	<b>82.0<math>\pm</math>5.3</b>
SF4	10 nodes			20 nodes			50 nodes		
	FDR	TPR	SHD	FDR	TPR	SHD	FDR	TPR	SHD
CD-NOD	0.36 $\pm$ 0.10	0.19 $\pm$ 0.02	25.0 $\pm$ 1.4	0.34 $\pm$ 0.05	0.18 $\pm$ 0.01	59.3 $\pm$ 0.9	0.38 $\pm$ 0.04	0.15 $\pm$ 0.01	168.3 $\pm$ 1.7
NOTEARS	<b>0.04<math>\pm</math>0.04</b>	0.81 $\pm$ 0.02	6.1 $\pm$ 1.1	0.19 $\pm$ 0.01	0.77 $\pm$ 0.02	27.1 $\pm$ 1.5	<b>0.17<math>\pm</math>0.01</b>	0.83 $\pm$ 0.01	60.7 $\pm$ 2.5
DAGGNN	0.07 $\pm$ 0.03	0.98 $\pm$ 0.02	2.9 $\pm$ 1.5	0.27 $\pm$ 0.03	0.84 $\pm$ 0.02	31.6 $\pm$ 2.6	0.26 $\pm$ 0.02	0.88 $\pm$ 0.01	80.6 $\pm$ 8.3
NoCurl	0.06 $\pm$ 0.02	0.86 $\pm$ 0.02	4.8 $\pm$ 1.1	0.25 $\pm$ 0.01	<b>0.86<math>\pm</math>0.01</b>	28.2 $\pm$ 1.3	0.26 $\pm$ 0.08	<b>0.93<math>\pm</math>0.05</b>	71.8 $\pm$ 10.6
DARING	0.17 $\pm$ 0.04	0.86 $\pm$ 0.07	9.0 $\pm$ 2.7	0.26 $\pm$ 0.02	0.80 $\pm$ 0.01	32.6 $\pm$ 1.8	0.28 $\pm$ 0.02	0.87 $\pm$ 0.01	87.3 $\pm$ 5.9
DICD	0.05 $\pm$ 0.04	<b>0.98<math>\pm</math>0.02</b>	<b>2.3<math>\pm</math>1.7</b>	<b>0.16<math>\pm</math>0.05</b>	0.81 $\pm$ 0.09	<b>22.1<math>\pm</math>8.4</b>	0.18 $\pm$ 0.03	0.91 $\pm$ 0.01	<b>53.7<math>\pm</math>8.7</b>

Table 3: Nonlinear Setting, for ER and SF graphs of 10, 20, 50 nodes

ER4	10 nodes			20 nodes			50 nodes		
	FDR	TPR	SHD	FDR	TPR	SHD	FDR	TPR	SHD
CD-NOD	0.39 $\pm$ 0.06	0.50 $\pm$ 0.07	20.0 $\pm$ 3.1	0.31 $\pm$ 0.04	0.56 $\pm$ 0.06	56.8 $\pm$ 4.2	0.35 $\pm$ 0.07	0.82 $\pm$ 0.05	115.7 $\pm$ 18.3
NOTEARS-MLP	0.24 $\pm$ 0.10	0.44 $\pm$ 0.12	23.8 $\pm$ 3.5	<b>0.25<math>\pm</math>0.05</b>	0.35 $\pm$ 0.09	59.0 $\pm$ 5.0	0.30 $\pm$ 0.08	0.86 $\pm$ 0.06	102.9 $\pm$ 25.4
DAGGNN	0.50 $\pm$ 0.06	0.21 $\pm$ 0.04	32.2 $\pm$ 1.5	0.61 $\pm$ 0.07	0.24 $\pm$ 0.05	82.9 $\pm$ 4.5	0.62 $\pm$ 0.06	0.15 $\pm$ 0.03	217.0 $\pm$ 16.0
NoCurl	0.38 $\pm$ 0.02	0.38 $\pm$ 0.05	27.4 $\pm$ 1.5	0.56 $\pm$ 0.07	0.34 $\pm$ 0.07	80.2 $\pm$ 7.6	0.69 $\pm$ 0.07	0.28 $\pm$ 0.07	258.2 $\pm$ 25.2
DARING	0.44 $\pm$ 0.04	0.28 $\pm$ 0.04	29.8 $\pm$ 2.7	0.55 $\pm$ 0.09	0.23 $\pm$ 0.07	77.6 $\pm$ 5.7	0.58 $\pm$ 0.09	0.23 $\pm$ 0.05	209.4 $\pm$ 20.0
DICD	<b>0.20<math>\pm</math>0.08</b>	<b>0.57<math>\pm</math>0.10</b>	<b>19.2<math>\pm</math>4.3</b>	0.26 $\pm$ 0.06	<b>0.69<math>\pm</math>0.07</b>	<b>40.3<math>\pm</math>6.1</b>	<b>0.26<math>\pm</math>0.04</b>	<b>0.88<math>\pm</math>0.03</b>	<b>84.4<math>\pm</math>11.7</b>
SF4	10 nodes			20 nodes			50 nodes		
	FDR	TPR	SHD	FDR	TPR	SHD	FDR	TPR	SHD
CD-NOD	0.42 $\pm$ 0.03	0.68 $\pm$ 0.04	19.5 $\pm$ 2.5	0.31 $\pm$ 0.09	0.64 $\pm$ 0.07	46.3 $\pm$ 6.8	0.32 $\pm$ 0.05	0.75 $\pm$ 0.09	104.3 $\pm$ 12.1
NOTEARS-MLP	0.41 $\pm$ 0.10	0.31 $\pm$ 0.16	25.2 $\pm$ 4.6	0.29 $\pm$ 0.10	0.56 $\pm$ 0.10	51.0 $\pm$ 7.4	0.29 $\pm$ 0.08	0.72 $\pm$ 0.13	113.7 $\pm$ 17.3
DAGGNN	0.62 $\pm$ 0.09	0.26 $\pm$ 0.07	31.2 $\pm$ 3.4	0.69 $\pm$ 0.07	0.16 $\pm$ 0.03	80.1 $\pm$ 7.4	0.64 $\pm$ 0.03	0.15 $\pm$ 0.05	210.3 $\pm$ 8.2
NoCurl	0.54 $\pm$ 0.06	0.40 $\pm$ 0.10	26.2 $\pm$ 2.0	0.70 $\pm$ 0.04	0.27 $\pm$ 0.05	87.2 $\pm$ 3.0	0.70 $\pm$ 0.02	0.22 $\pm$ 0.01	240.8 $\pm$ 9.3
DARING	0.54 $\pm$ 0.10	0.27 $\pm$ 0.05	29.0 $\pm$ 2.7	0.58 $\pm$ 0.06	0.21 $\pm$ 0.03	73.1 $\pm$ 4.5	0.53 $\pm$ 0.03	0.19 $\pm$ 0.02	193.0 $\pm$ 5.0
DICD	<b>0.34<math>\pm</math>0.06</b>	<b>0.71<math>\pm</math>0.15</b>	<b>16.2<math>\pm</math>4.3</b>	<b>0.27<math>\pm</math>0.06</b>	<b>0.68<math>\pm</math>0.15</b>	<b>37.9<math>\pm</math>7.1</b>	<b>0.29<math>\pm</math>0.04</b>	<b>0.80<math>\pm</math>0.03</b>	<b>99.3<math>\pm</math>9.0</b>

### 5.1.1 Datasets

We conduct experiments on two synthetic datasets for linear and nonlinear settings. Besides, we apply our method DICD on Colored MNIST [7] dataset to explore its effectiveness on real-world datasets. As for the synthetic data, the ground truth DAG is generated from two random graph models: Erdos-Renyi (ER) and scale-free (SF), following [52]. For the overall experimental comparison, we set the node degree as four. For the linear and nonlinear setting, we construct the environment variable  $E$  to simulate the effects of the environments on the additive noises. The detailed generation process could be found Appendix D.1. Finally, for the real-world dataset, we sampled 10000 images from the MNIST dataset. The details of CMNIST are provided in Appendix D.5.

### 5.2 Overall Performances (RQ1)

We present the overall performances of DICD and the baselines for fair comparison. In the baselines, NOTEARS, DAGGNN, NoCurl, DARING are run on the concatenated datasets from all the environments. CD-NOD is run with the environment-id corresponding to each sample.

#### 5.2.1 Linear Synthetic Data

In this experiment, we explore the improvements when introducing different groups by comparing the DAG estimations against the ground truth structure. We simulate {ER4, SF4} graphs with  $d = \{10, 20, 50, 100\}$  nodes. For each environment, we generate 200 samples. We evaluate our methods with datasets from 5 environments, and the variances of Gaussian noise for the environment variable  $E$  in each environment are  $\{0.2, 0.4, 0.6, 0.8, 1.0\}$ . Table 2 summarizes the results when the number of nodes equals to  $\{10, 20, 50\}$ , and the results of node number 100 are provided in Appendix E.1. From these tables, we could have the following key observations: (1) DICD has outperformed all other baselines across various settings. More precisely, DICD achieves significant improvements over the strongest baselines by up to 36% in SHD (10 nodes, ER graph). (2) Generally, DICD has the lower FDR and higher TPR, which also coincides with the intuition that DICD could eliminate spurious correlations and reveal the true ones.

#### 5.2.2 Nonlinear Synthetic Data

We also conduct enormous experiments to demonstrate the effectiveness of DICD in the nonlinear setting. Similarly to the linear setting, we simulate {ER4, SF4} graphs with  $d = \{10, 20, 50, 100\}$

nodes. For each graph, we generate data from two environments, 1000 samples for each environment. The Gaussian noises for the environment variable  $E$  in these two groups are  $\{0.2, 0.4\}$ . The results with  $d = \{10, 20, 50\}$  are provided in Table 3 and results with  $d = 100$  are shown in Appendix E.1. From these tables, we could find: (1) DICD consistently outperforms other baselines in all eight settings upon the most crucial metric SHD. The improvements on SHD over the best baseline are up to 29% (50 nodes, ER graph). (2) DICD achieves compatible FDR with NOTEARS but far higher TPR. This shows that in the nonlinear setting, DICD is better at revealing the true causal correlations that might have been missed by NOTEARS. (3) The over-reconstruction problem still exists in other methods, while DICD has the potential to mitigate it, which could be the reason for the performance improvements. (4) CD-NOD performs fairly well in nonlinear cases, which means the multi-environment setting might be more helpful when the correlations between variables are more complicated. However, CD-NOD consumes in average more than 9 hours in the simplest setting (10 nodes), and more than 200 hours in the case of 50 nodes, which is far more expensive than our algorithm (see Appendix E.1.2).

### 5.3 Study of various factors (RQ2)

In this section, we discuss various factors that may affect the performances of DICD and other methods. Due to limit of space, we discuss the effect of environmental imbalance in Appendix E.1.1.

### 5.3.1 The effect of the number of environments

To explore how the number of environments affects the performances, we conduct experiments on both linear and nonlinear settings. The total number of the examples is set to 1000. We choose  $d = 10$  and  $s_0 = 40$  with ER graph for this case study. If the number of the environments is  $N$ , then the number of samples for each environment is  $\lfloor 1000/N \rfloor$ . The noises for different environments are sliced from the head of the array  $\{0.2, 0.4, 0.6, 0.8, 1.0, 0.1, 0.3, 0.5, 0.7, 0.9\}$ . For example, the noises are  $\{0.2, 0.4\}$  when the number of environments is 2. In Figure 1, we can observe: (1) When the number of environments is greater than 4 in the linear setup, more environments will not yield to better results, which means for simple structure equation models, four environments may have already ruled out the possibility of incorrect graphs. (2) In the nonlinear setting, it is amazing to find that DICD could achieve better performance even there is only one environment. The reason could be that when there are more parameters in the function, the explicit constraint on the optimality of the parameters could contribute much to learning the best graph, which is more likely to be the ground truth graph. (3) More environments in nonlinear settings could degrade the performance of all approaches; the reason for this could be that heterogeneous noises can be particularly unfriendly when the relationships between variables become quite intricate.

Figure 1 consists of two line plots, (a) Linear Setting and (b) Nonlinear Setting, showing the relationship between the Number of Environments (1 to 10) and the SHD (0 to 35). The legend for both plots includes: NOTEARS (light blue), DAGNN (orange), DARING (green), NoCurl (dark blue), and DICD (red). In the Linear Setting plot, SHD generally decreases as the number of environments increases, with DICD showing the lowest SHD for N > 4. In the Nonlinear Setting plot, SHD is generally higher and more variable, with DICD showing the lowest SHD for N > 4.

Number of Environments	Linear Setting (SHD)	Nonlinear Setting (SHD)
1	13.5	28.0
2	12.5	25.0
4	9.5	28.0
6	10.5	28.0
8	10.0	35.0
10	10.5	28.0

(a) Linear Setting (b) Nonlinear Setting

Figure 1: SHD w.r.t. the number of environments.

### 5.3.2 The effect of the density of the graph

We aim to discover how much the node degree (*i.e.*, density) will affect our algorithm compared to the other baselines. We choose SF graph with  $d = 20$  for this case study. In the linear setting, we generate samples from five environments, 200 samples for each. And for nonlinear settings, we draw samples from two environments, 1000 samples for each. The x-axis represents the mean degree of the nodes in the generated graph. For instance, Node degree = 10 means there are 200 edges in total when generating the DICD almost consistently outperforms the other baselines (*i.e.*, the density) increases, especially in baselines get larger, which means DICD could be

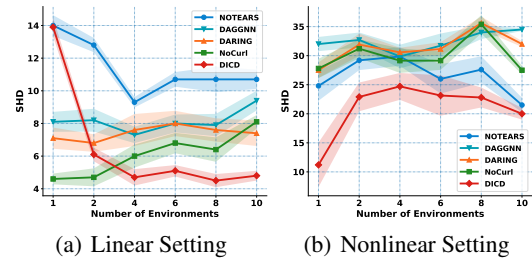


Figure 1: SHD w.r.t. the number of environments.

(3) More environments in nonlinear settings could be a reason for this because heterogeneous noises can make the relationships between variables become quite intricate.

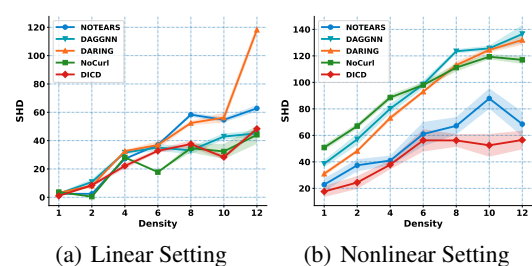


Figure 2: SHD for different density conditions.

the SF graph. from Figure 2, we could observe: (1) our methods, except for few cases. (2) As the node nonlinear settings, the improvements of DICD over SCD better adapt to the denser settings.

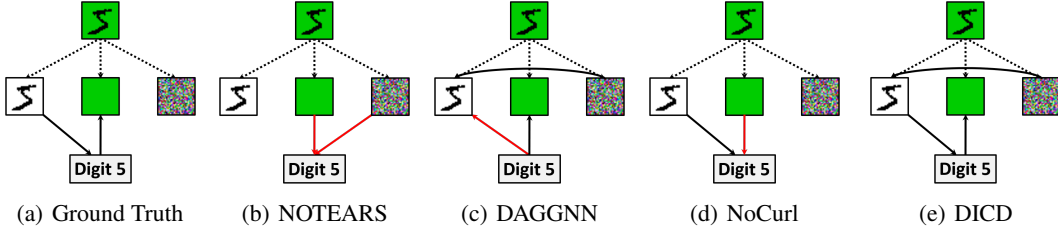


Figure 3: Revealed graph by different methods on Real World Data

#### 5.4 Real data (RQ3)

Finally, we evaluate our method on the real-world data: ColoredMNIST. Our method, as well as NOTEARS-MLP, could be simply extended to the setting of vector-valued variable. DAG-GNN is already designed to work in this situation. However, DARING do not discuss this situation in the paper. Though it seems that DARING could also be generalized to vector-valued, efforts need to be taken. Thus we omit it as comparison in this section. As stated earlier in Section 5.1.1, we sample 10000 images from the MNIST dataset and generate the colored version of MNIST. In the pictures, we have kept the digits to be black, while the background has the color red or green. The images are resized to 8\*8, and then flattened to yield a 64-dim vector. The label vector and color vector are set to be all zeros or all ones (according to the original label) with dimension as 64. Then during searching (or training) we only consider the possible correlations among the white backgrounds, colors, noises, and digits. Thus we have four variables in the designed task. As shown in Figure 3. We could find NOTEARS, DAGGNN and NoCurl all make mistakes, while DICD gives reasonable predictions.

## 6 Related Work

Causal Discovery has caught enormous attention recently. We will mainly discuss the differentiable score-based algorithms and the works considering multi-environments.

**Differentiable Score-based algorithms.** Score-based causal discovery methods aim to find the causal structure by optimizing a carefully defined score function via various modelling methods. Though there are conventional methods [14, 43, 8, 27, 35] applying various techniques such as hill-climbing[49] and integer programming [23], the differentiable methods using gradient descent show stronger power. NOTEARS [51] reformulate the causal discovery problem with acyclicity constraint as a continuous program. DAG-GNN [47] proposes a variant of the acyclicity constraint and solves the generalized linear SEM in a graph autoencoder structure. NOTEARS-MLP [52] and GraN-DAG [21] extend the continuous acyclicity regularization into a neural network and achieve better results in the nonlinear settings. RL-BIC [53] introduces RL to find the DAG with the best BIC score. DARING [13] proposes to constrain the independence between the residuals and adopts an adversarial training strategy. DAG-GAN [10] formulates the problem of DAG structure learning from the perspective of distributional optimization. [24] shows that applying soft sparsity and DAG constraints would be enough. There are also other works that apply some alternatives of the continuous acyclicity regularization. DAG-NoCurl [48] aims at eliminating the DAG constraint entirely, by showing that the set of weighted adjacency matrices of DAGs are equivalent to the set of weighted gradients of graph potential functions. NODAG [45] proposes to solve an  $l_1$ -penalized optimization, while ENCO [22] provides convergence guarantees without constraining the score function with respect to acyclicity. These methods all have their own strategies to control the acyclicity.

**Previous work considering multi-environments.** Most work with multi-environment settings are built on constraint-based methods [38, 39, 17, 50, 37]. Although they achieved lots of improvements, there are some major limitations: 1) may have overly strict domain definition [30]; 2) limited to linear cases only [11, 15, 12]; 3) designed to solve much simpler problems than CD such as causal direction identification [15, 5]; 4) may involve a large number of independence tests and be very time-consuming [11, 16], which is also the general problem of constraint-based methods. However, We define the environments following [1, 11, 12], and our method is capable of solving the general causal discovery problems in both linear and nonlinear cases. There is another interesting and more general task called Federated Causal Discovery [9, 25, 40, 42, 41], which aims to solve the problem about decentralized datasets. Though our targets are different, the algorithms are somewhat similar.

## 7 Conclusion and Future Work

Despite the great success in causal structure learning, today’s differentiable causal discovery methods are still suffering from non-identifiability issue and over-reconstruction problem. In this paper, we proposed a simple yet effective Differentiable Invariant Causal Discovery (DICD) method to tackle the challenge by incorporating the multi-environment information. Our main idea is that, given the true causal graph, the parameters of SEM learned from different environments should remain consistent. Theoretical guarantees for the identifiability of proposed DICD are provided under certain assumptions about the environments. The extensive experimental results demonstrate the effectiveness of DICD. The limitation of DICD is that we need the environment information. In the future, we may consider discovering environments from the dataset, *i.e.*, environment inferring. Without the strict requirement of knowing the environment information in advance, our algorithm will be applicable in more general scenarios.

## References

- [1] Martín Arjovsky, Léon Bottou, Ishaan Gulrajani, and David Lopez-Paz. Invariant risk minimization. *CoRR*, 2019.
- [2] Peter Bandi, Oscar Geessink, Quirine Manson, Marcory Van Dijk, Maschenka Balkenhol, Meyke Hermsen, Babak Ehteshami Bejnordi, Byungjae Lee, Kyunghyun Paeng, Aoxiao Zhong, et al. From detection of individual metastases to classification of lymph node status at the patient level: the camelyon17 challenge. *IEEE Transactions on Medical Imaging*, 2018.
- [3] Rohit Bhattacharya, Tushar Nagarajan, Daniel Malinsky, and Ilya Shpitser. Differentiable causal discovery under unmeasured confounding. In *AISTATS*, pages 2314–2322. PMLR, 2021.
- [4] Rémi Cadène, Corentin Dancette, Hedi Ben-younes, Matthieu Cord, and Devi Parikh. Rubi: Reducing unimodal biases in visual question answering. *CoRR*, abs/1906.10169, 2019.
- [5] Ruichu Cai, Jincheng Ye, Jie Qiao, Huiyuan Fu, and Zhifeng Hao. FOM: fourth-order moment based causal direction identification on the heteroscedastic data. *Neural Networks*, 124:193–201, 2020.
- [6] Jia Deng, Wei Dong, Richard Socher, Li-Jia Li, Kai Li, and Li Fei-Fei. Imagenet: A large-scale hierarchical image database. In *CVPR*, pages 248–255, 2009.
- [7] Li Deng. The mnist database of handwritten digit images for machine learning research. *IEEE Signal Processing Magazine*, 29(6):141–142, 2012.
- [8] José A. Gámez, Juan L. Mateo, and José Miguel Puerta. Learning bayesian networks by hill climbing: efficient methods based on progressive restriction of the neighborhood. *Data Min. Knowl. Discov.*, 22(1-2):106–148, 2011.
- [9] Erdun Gao, Junjia Chen, Li Shen, Tongliang Liu, Mingming Gong, and Howard Bondell. Federated causal discovery. *CoRR*, abs/2112.03555, 2021.
- [10] Yinghua Gao, Li Shen, and Shu-Tao Xia. Dag-gan: Causal structure learning with generative adversarial nets. In *ICASSP 2021-2021 IEEE International Conference on Acoustics, Speech and Signal Processing (ICASSP)*, pages 3320–3324. IEEE, 2021.
- [11] AmirEmad Ghassami, Negar Kiyavash, Biwei Huang, and Kun Zhang. Multi-domain causal structure learning in linear systems. In *NeurIPS*, pages 6269–6279, 2018.
- [12] AmirEmad Ghassami, Saber Salehkaleybar, Negar Kiyavash, and Kun Zhang. Learning causal structures using regression invariance. In *NIPS*, pages 3011–3021, 2017.
- [13] Yue He, Peng Cui, Zheyuan Shen, Renzhe Xu, Furui Liu, and Yong Jiang. DARING: differentiable causal discovery with residual independence. In *KDD*, pages 596–605, 2021.
- [14] David Heckerman, Dan Geiger, and David Maxwell Chickering. Learning bayesian networks: The combination of knowledge and statistical data. *Mach. Learn.*, 20(3):197–243, 1995.

[15] Biwei Huang, Kun Zhang, Mingming Gong, and Clark Glymour. Causal discovery and forecasting in nonstationary environments with state-space models. In *ICML*, volume 97 of *Proceedings of Machine Learning Research*, pages 2901–2910. PMLR, 2019.

[16] Biwei Huang, Kun Zhang, Jiji Zhang, Joseph D. Ramsey, Ruben Sanchez-Romero, Clark Glymour, and Bernhard Schölkopf. Causal discovery from heterogeneous/nonstationary data. *J. Mach. Learn. Res.*, 21:89:1–89:53, 2020.

[17] Biwei Huang, Kun Zhang, Jiji Zhang, Joseph D Ramsey, Ruben Sanchez-Romero, Clark Glymour, and Bernhard Schölkopf. Causal discovery from heterogeneous/nonstationary data. *J. Mach. Learn. Res.*, 21(89):1–53, 2020.

[18] Gary B Huang, Marwan Mattar, Tamara Berg, and Eric Learned-Miller. Labeled faces in the wild: A database for studying face recognition in unconstrained environments. In *Workshop on faces in 'Real-Life' Images: detection, alignment, and recognition*, 2008.

[19] Pang Wei Koh, Shiori Sagawa, Sang Michael Xie, Marvin Zhang, Akshay Balsubramani, Weihua Hu, Michihiro Yasunaga, Richard Lanas Phillips, Irena Gao, Tony Lee, et al. Wilds: A benchmark of in-the-wild distribution shifts. In *International Conference on Machine Learning*, pages 5637–5664. PMLR, 2021.

[20] David Krueger, Ethan Caballero, Jörn-Henrik Jacobsen, Amy Zhang, Jonathan Binas, Dinghuai Zhang, Rémi Le Priol, and Aaron C. Courville. Out-of-distribution generalization via risk extrapolation (rex). In *ICML*, volume 139, pages 5815–5826, 2021.

[21] Sébastien Lachapelle, Philippe Brouillard, Tristan Deleu, and Simon Lacoste-Julien. Gradient-based neural DAG learning. In *ICLR*. OpenReview.net, 2020.

[22] Phillip Lippe, Taco Cohen, and Efstratios Gavves. Efficient neural causal discovery without acyclicity constraints. *arXiv preprint arXiv:2107.10483*, 2021.

[23] Hasan Manzour, Simge Küçükayuz, and Ali Shojaie. Integer programming for learning directed acyclic graphs from continuous data. *CoRR*, abs/1904.10574, 2019.

[24] Ignavier Ng, AmirEmad Ghassami, and Kun Zhang. On the role of sparsity and dag constraints for learning linear dags. *arXiv preprint arXiv:2006.10201*, 2020.

[25] Ignavier Ng and Kun Zhang. Towards federated bayesian network structure learning with continuous optimization. *CoRR*, abs/2110.09356, 2021.

[26] Jianmo Ni, Jiacheng Li, and Julian McAuley. Justifying recommendations using distantly-labeled reviews and fine-grained aspects. In *Proceedings of the 2019 Conference on Empirical Methods in Natural Language Processing and the 9th International Joint Conference on Natural Language Processing (EMNLP-IJCNLP)*, 2019.

[27] Siqi Nie, Denis Deratani Mauá, Cassio P. de Campos, and Qiang Ji. Advances in learning bayesian networks of bounded treewidth. In *NIPS*, pages 2285–2293, 2014.

[28] Rainer Opgen-Rhein and Korbinian Strimmer. From correlation to causation networks: a simple approximate learning algorithm and its application to high-dimensional plant gene expression data. *BMC systems biology*, 1(1):1–10, 2007.

[29] Judea Pearl, Madelyn Glymour, and Nicholas P Jewell. *Causal inference in statistics: A primer*. John Wiley & Sons, 2016.

[30] Jonas Peters, Peter Bühlmann, and Nicolai Meinshausen. Causal inference by using invariant prediction: identification and confidence intervals. *Journal of the Royal Statistical Society: Series B (Statistical Methodology)*, 78(5):947–1012, 2016.

[31] Jie Qiao, Yiming Bai, Ruichu Cai, and Zhifeng Hao. Causal discovery from multi-domain data using the independence of modularities. *Neural Comput. Appl.*, 34(3):1939–1949, 2022.

[32] Karen Sachs, Omar Perez, Dana Pe'er, Douglas A Lauffenburger, and Garry P Nolan. Causal protein-signaling networks derived from multiparameter single-cell data. *Science*, 308(5721):523–529, 2005.

[33] Shiori Sagawa, Pang Wei Koh, Tatsunori B. Hashimoto, and Percy Liang. Distributionally robust neural networks for group shifts: On the importance of regularization for worst-case generalization. *ICLR*, 2019.

[34] Andrew D Sanford and Imad A Moosa. A bayesian network structure for operational risk modelling in structured finance operations. *Journal of the Operational Research Society*, 63(4):431–444, 2012.

[35] Mauro Scanagatta, Cassio P. de Campos, Giorgio Corani, and Marco Zaffalon. Learning bayesian networks with thousands of variables. In *NIPS*, pages 1864–1872, 2015.

[36] Patrick Schwab and Walter Karlen. Cexplain: Causal explanations for model interpretation under uncertainty. In *NeurIPS*, pages 10220–10230, 2019.

[37] Ram Shanmugam. Causality: Models, reasoning, and inference : Judea pearl; cambridge university press, cambridge, uk, 2000, pp 384, ISBN 0-521-77362-8. *Neurocomputing*, 41(1-4):189–190, 2001.

[38] Peter Spirtes, Clark N Glymour, Richard Scheines, and David Heckerman. *Causation, prediction, and search*. MIT press, 2000.

[39] Peter L Spirtes, Christopher Meek, and Thomas S Richardson. Causal inference in the presence of latent variables and selection bias. *arXiv preprint arXiv:1302.4983*, 2013.

[40] Robert E. Tillman, David Danks, and Clark Glymour. Integrating locally learned causal structures with overlapping variables. In *NIPS*, pages 1665–1672. Curran Associates, Inc., 2008.

[41] Sofia Triantafillou and Ioannis Tsamardinos. Constraint-based causal discovery from multiple interventions over overlapping variable sets. *J. Mach. Learn. Res.*, 16:2147–2205, 2015.

[42] Sofia Triantafillou, Ioannis Tsamardinos, and Ioannis G. Tollis. Learning causal structure from overlapping variable sets. In *AISTATS*, volume 9 of *JMLR Proceedings*, pages 860–867. JMLR.org, 2010.

[43] Ioannis Tsamardinos, Laura E Brown, and Constantin F Aliferis. The max-min hill-climbing bayesian network structure learning algorithm. *Machine learning*, 65(1):31–78, 2006.

[44] Vladimir Vapnik. Principles of risk minimization for learning theory. In *NeurIPS*, pages 831–838, 1991.

[45] Gherardo Varando. Learning dags without imposing acyclicity. *arXiv preprint arXiv:2006.03005*, 2020.

[46] Minh N. Vu and My T. Thai. Pgm-explainer: Probabilistic graphical model explanations for graph neural networks. In *NeurIPS*, 2020.

[47] Yue Yu, Jie Chen, Tian Gao, and Mo Yu. DAG-GNN: DAG structure learning with graph neural networks. In *ICML*, volume 97, pages 7154–7163, 2019.

[48] Yue Yu and Tian Gao. Dags with no curl: Efficient dag structure learning. In *Causal Discovery & Causality-Inspired Machine learning Workshop at 34th Conference on Neural Information-Processing Systems (NeurIPS 2020)*, 2020.

[49] Changhe Yuan and Brandon M. Malone. Learning optimal bayesian networks: A shortest path perspective. *J. Artif. Intell. Res.*, 48:23–65, 2013.

[50] Hao Zhang, Kun Zhang, Shuigeng Zhou, Jihong Guan, and Ji Zhang. Testing independence between linear combinations for causal discovery. In *Proceedings of the AAAI Conference on Artificial Intelligence*, volume 35, pages 6538–6546, 2021.

[51] Xun Zheng, Bryon Aragam, Pradeep Ravikumar, and Eric P. Xing. Dags with NO TEARS: continuous optimization for structure learning. In *NeurIPS*, pages 9492–9503, 2018.

- [52] Xun Zheng, Chen Dan, Bryon Aragam, Pradeep Ravikumar, and Eric P. Xing. Learning sparse nonparametric dags. In *AISTATS*, volume 108, pages 3414–3425, 2020.
- [53] Shengyu Zhu, Ignavier Ng, and Zhitang Chen. Causal discovery with reinforcement learning. In *ICLR*, 2020.

## A Notations

Table 4 provides the meanings of all the notations used in the main paper.

Table 4: Notations and the corresponding Meanings

Notations	Meanings
$n$	number of the data samples
$d$	number of the variables (or nodes)
$\mathbf{X}$	$\mathbb{R}^{n \times d}$ , observational data
$\mathbf{x}_j$	$\mathbb{R}^n$ , observational data corresponding to the $j$ -th variable
$X_j$	$j$ -th node variable
$F$	ground truth structure function
$F_j$	ground truth structure function corresponding to $X_j$
$f$	estimated structure function
$f_j$	estimated structure function corresponding to $X_j$
$\text{Pa}(X_j)$	parent set of $X_j$
$\text{Pa}(j)$	the index set of the parents of $X_j$
$z_j$	additive noise of $X_j$
$\sigma_z^2$	variance of $z_j$
$\mathcal{G}(\cdot)$	corresponding graph of $\cdot$
$\mathbf{W}$	$\mathbb{R}^{d \times d}$ , the coefficients for all edges of $\mathcal{G}(f)$ in linear situations
$m_l$	the number of hidden units in the $l$ -th layer in MLP
$\mathbf{S}$	$\{0, 1\}^{d \times d}$ invariant structure model

## B Basic Structure Example

Table 5: The specific confounder case in which NOTEARS[51] might make mistakes. Detailed data generation processes are as follows. Environment 1:  $A = z_A(\sim \mathcal{N}(0, 4))$ ,  $B = A/2 + z_B(\sim \mathcal{N}(0, 1))$ ,  $C = A + B/2 + z_C(\sim \mathcal{N}(0, 4))$ . Environment 2:  $A = z_A(\sim \mathcal{N}(0, 4))$ ,  $B = A/2 + z_B(\sim \mathcal{N}(0, 4))$ ,  $C = A + B/2 + z_C(\sim \mathcal{N}(0, 1))$ . Note that only the variance of  $z_B$  is different in two environments.

$e_1$	6.00(1.00, 0.50, 0.50)	6.05(0.00, 1.25, 0.40)	8.97(0.00, 0.67, 0.40)	5.67(0.00, 0.67, 1.50)	8.97(0.00, 0.67, 0.40)	5.00(1.00, 1.00, 0.50)
$e_2$	9.00(1.00, 0.50, 0.50)	8.00(-0.75, 1.25, 1.00)	11.22(-0.75, 0.61, 1.00)	9.96(-0.29, 0.76, 0.90)	11.56(-0.29, 0.76, 0.55)	9.20(0.40, 1.00, 0.50)

In this section, we provide another example shown in Table 5 to demonstrate our motivation introduced in Section 1. In this table, the blue graphs denote the ground truth, while graphs with red edges are the wrong edges in the wrong structures. Below the structures, the first number in front of the parenthesis refers to the least reconstruction loss( $\|\mathbf{XW} - \mathbf{X}\|_2$ ) given the structure in the same column of Table 5. Given the structure, we can use the structure to constrain which of the elements in  $\mathbf{W}$  should be non-zero elements and others are not. Then we can learn the optimal parameters for these non-zero elements. As shown in the Table, the numbers in the parenthesis refer to the optimal parameters for the edges between A-B, B-C, A-C, respectively. From this table, we can find that with wrong causal structures which have the potential to obtain lower reconstruction loss (*i.e.*, over-reconstruction), the parameters learned given these structures are not consistent across different environments. Thus with the condition given by DICD, we can rule out wrong graphs.

## C Definitions and Proofs of Theorems

### C.1 Definitions

**Definition C.1.** We define the node in the graph with no parents as the *Source Node*.

## C.2 Proof of Theorem 3.2

The basic optimality condition for Eq.(10) can be described as:

$$\mathbf{A}^* = \arg \min_{\mathbf{A}} \mathcal{L}^e(\mathbf{S} \circ \mathbf{A}), \text{ s.t. } \mathcal{G}(\mathbf{S}) = \mathcal{G}(\mathbf{A}) \in \text{DAG}. \quad (20)$$

Then we introduce a new matrix variable  $\mathbf{B}$  and insert it into Eq.(20) to define its optimal value as:

$$\mathbf{B}^* = \arg \min_{\mathbf{B}} \mathcal{L}^e(\mathbf{S} \circ \mathbf{A}^* \circ \mathbf{B}). \quad (21)$$

We assert  $\mathbf{B}^*$  could be the all-one matrix  $\mathbf{1}$ , which indicates:

$$\mathcal{L}^e(\mathbf{S} \circ \mathbf{A}^* \circ \mathbf{1}) \leq \mathcal{L}^e(\mathbf{S} \circ \mathbf{A}^* \circ \mathbf{B}), \quad \forall \mathbf{B} \in \mathbb{R}^{D \times D}. \quad (22)$$

Assuming there exists  $\mathbf{B}'$  that satisfies:

$$\mathcal{L}^e(\mathbf{S} \circ \mathbf{A}^* \circ \mathbf{B}') < \mathcal{L}^e(\mathbf{S} \circ \mathbf{A}^* \circ \mathbf{1}), \quad (23)$$

then we could replace  $\mathbf{A}^* \circ \mathbf{B}'$  with  $\mathbf{A}'$  and have:

$$\mathcal{L}^e(\mathbf{S} \circ \mathbf{A}') < \mathcal{L}^e(\mathbf{S} \circ \mathbf{A}^*), \quad (24)$$

which contradicts with Eq.(20). As such, Eq.(22) holds. We replace  $\mathbf{S} \circ \mathbf{A}$  with  $\mathbf{A}_S$ , and replace the matrix variable  $\mathbf{B}$  with  $\mathbf{A}$ , which could yield:

$$\mathbf{1} = \arg \min_{\mathbf{A}} \mathcal{L}^e(\mathbf{A}_S \circ \mathbf{A}). \quad (25)$$

According to KKT condition, we have:

$$\frac{\partial \mathcal{L}^e(\mathbf{A}_S \circ \mathbf{A})}{\partial \mathbf{A}} \Big|_{\mathbf{A}=\mathbf{1}} = \mathbf{0} \quad (26)$$

Then we arrive at Eq.(13).

## C.3 Proof of Theorem 3.3

The basic optimal condition described in Eq.(10) could be written as:

$$\mathbf{A}_i^{(1)*} = \arg \min_{\mathbf{A}_i^{(1)}} \mathcal{L}^e(\text{MLP}(\text{Re}([\mathbf{S}]_i, m_1) \circ \mathbf{A}_i^{(1)}, \dots, \mathbf{A}_i^{(n)})) \quad (27)$$

where  $\text{Re}([\mathbf{S}]_i, m_1)$  means  $\underbrace{[\mathbf{S}]_i, \dots, [\mathbf{S}]_i}_{m_1 \text{ times}}^\top$ , with  $[\mathbf{S}]_i$  being the  $i$ -th column of  $\mathbf{S}$ .

Similar to the proof of Proposition 3.2, we define a new matrix  $\mathbf{B} \in \mathbb{R}^{m_1 \times d}$ , and insert this term into Eq.(27), then we can have:

$$\mathbf{B}^* = \arg \min_{\mathbf{B}} \mathcal{L}^e(\text{MLP}(\text{Re}([\mathbf{S}]_i, m_1) \circ \mathbf{A}_i^{(1)*} \circ \mathbf{B}, \dots, \mathbf{A}_i^{(n)})) \quad (28)$$

We argue that  $\mathbf{B}^*$  could be  $\mathbf{1}$ , a matrix which has the same dimension as  $\mathbf{B}^*$  but filled with ones. This could be expresses as:

$$\mathbf{1} = \arg \min_{\mathbf{B}} \mathcal{L}^e(\text{MLP}(\text{Re}([\mathbf{S}]_i, m_1) \circ \mathbf{A}_i^{(1)*} \circ \mathbf{B}, \dots, \mathbf{A}_i^{(n)})) \quad (29)$$

Then replacing  $\text{Re}([\mathbf{S}]_i, m_1) \circ \mathbf{A}_i^{(1)*}$  with  $\mathbf{A}_{S_i}$  would yield:

$$\mathbf{1} = \arg \min_{\mathbf{B}} \mathcal{L}^e(\text{MLP}(\mathbf{A}_{S_i} \circ \mathbf{B}, \mathbf{A}_i^{(2)}, \dots, \mathbf{A}_i^{(n)})) \quad (30)$$

Still with KKT condition, we can have Eq.(28).

#### C.4 Proof of Theorem 4.1

To begin with, we provide the notations used in this proof. We denote the set of all variables as  $\{X_1, \dots, X_d\}$ , and the vector variable  $[X_1, \dots, X_d]^\top$  is denoted as  $\mathbf{X}$  in this section. The set of parent nodes of  $X_i$  is denoted as  $Pa(X_i)$ , while the index set of  $Pa(X_i)$  is denoted as  $Pa(i)$ .

First of all, we propose the following Lemma C.2 to show that our DICD could yield the true coefficient in linear systems under the true causal structure.

**Lemma C.2.** *Given the true graph  $G_0$ , the corresponding structure  $\mathbf{S}_0$  is the adjacency matrix of  $G_0$ .  $\forall e \in \mathcal{E}$ , we denote the the optimal parameters for the coefficients in environment  $e$  as  $\hat{\mathbf{W}}^e$ :*

$$\hat{\mathbf{W}}^e = \arg \min_{\bar{\mathbf{W}}} \mathcal{L}^e(\mathbf{S}_0 \circ \bar{\mathbf{W}}), \quad \text{s.t. } \mathcal{G}(\mathbf{S}_0) = \mathcal{G}(\bar{\mathbf{W}}) \quad (31)$$

Then we have  $\hat{\mathbf{W}}^e = \mathbf{W}_0, \forall e \in \mathcal{E}$ , where  $\mathbf{W}_0$  means the ground truth coefficients.

*Proof.* We consider the linear regression coefficient  $\hat{\mathbf{W}}^e$  for every environment  $e$ . The regression process in Eq.(31) is equivalent to performing the regression for every node  $X_m, m \in \{1, \dots, d\}$  from its parents  $Pa(X_m)$ .

We incorporate the environment information into the expectation operator  $\mathbb{E}_e$ . The coefficients of the node  $X_m$  is denoted as:

$$[\hat{\mathbf{W}}^e]_m = \arg \min_{\bar{\mathbf{W}}} \mathbb{E}_e \|X_m - (\bar{\mathbf{W}} \circ [\mathbf{S}_0]_m)^\top \mathbf{X}\| \quad (32)$$

where  $[\hat{\mathbf{W}}^e]_m$  represents the  $m$ -th column of  $[\hat{\mathbf{W}}^e]$  and  $[\mathbf{S}_0]_m$  is the  $m$ -th column of  $[\mathbf{S}_0]$ . Then we can further express  $[\hat{\mathbf{W}}^e]_m$  in Eq.(32) as:

$$[\hat{\mathbf{W}}^e]_m = \mathbb{E}_e [X_m \left( ([\mathbf{S}_0]_m \circ \mathbf{X}) ([\mathbf{S}_0]_m \circ \mathbf{X})^\top \right)^{-1} [\mathbf{S}_0]_m \circ \mathbf{X}] \quad (33)$$

For simplicity, we denote  $[\mathbf{S}_0]_m \circ \mathbf{X}$  as  $\mathbf{X}_{\mathbf{S}_0 m}$ .

We extract the  $m$ -th column of  $\mathbf{W}_0$  as  $[\mathbf{W}_0]_m$ , and the true generation process for  $X_m$  could be expressed as:

$$X_m = [\mathbf{W}_0]_m^\top \mathbf{X} + z_m \quad (34)$$

where  $z_m \sim \mathcal{N}(0, (\sigma_m^e)^2)$ . Then as  $[\mathbf{W}_0]$  is the ground truth coefficients,  $[\mathbf{W}_0]$  should be consistent with the graph  $G_0$ , as well as the structure  $\mathbf{S}_0$ . Thus we have:  $\mathbf{W}_0 = \mathbf{S}_0 \circ \mathbf{W}_0$ , which indicates  $[\mathbf{W}_0]_m^\top \mathbf{X} = [\mathbf{S}_0]_m \circ [\mathbf{W}_0]_m^\top \mathbf{X} = [\mathbf{W}_0]_m^\top \mathbf{X}_{\mathbf{S}_0 m}$ . Thus the generation process in Eq.(34) could be rewritten as:

$$X_m = [\mathbf{W}_0]_m^\top \mathbf{X}_{\mathbf{S}_0 m} + z_m \quad (35)$$

Then we can substitute Eq.(35) into Eq.(32) to obtain:

$$[\hat{\mathbf{W}}^e]_m = \mathbb{E}_e [([\mathbf{W}_0]_m^\top \mathbf{X}_{\mathbf{S}_0 m} + z_m) (\mathbf{X}_{\mathbf{S}_0 m} (\mathbf{X}_{\mathbf{S}_0 m})^\top)^{-1} \mathbf{X}_{\mathbf{S}_0 m}] \quad (36)$$

Since  $z_m$  is an independent additive noise, we can remove  $z_m$  in the above equation and yield:

$$\begin{aligned} [\hat{\mathbf{W}}^e]_m &= \mathbb{E}_e [([\mathbf{W}_0]_m^\top \mathbf{X}_{\mathbf{S}_0 m}) (\mathbf{X}_{\mathbf{S}_0 m} (\mathbf{X}_{\mathbf{S}_0 m})^\top)^{-1} \mathbf{X}_{\mathbf{S}_0 m}] \\ &= \mathbb{E}_e [(\mathbf{X}_{\mathbf{S}_0 m} (\mathbf{X}_{\mathbf{S}_0 m})^\top)^{-1} \mathbf{X}_{\mathbf{S}_0 m} \mathbf{X}_{\mathbf{S}_0 m}^\top] [\mathbf{W}_0]_m^\top = [\mathbf{W}_0]_m^\top \end{aligned} \quad (37)$$

Note that  $[\mathbf{W}_0]_m^\top \mathbf{X}_{\mathbf{S}_0 m}$  is a scalar. We adopt the rule  $(\mathbf{a} \cdot \mathbf{b})\mathbf{c} = (\mathbf{c} \cdot \mathbf{b}^\top) \cdot \mathbf{a}$ , where  $\mathbf{a}, \mathbf{b}, \mathbf{c}$  are vectors of the same dimension in the second line. Moreover, since  $[\mathbf{W}_0]_m^\top$  is independent of the environment  $e$  and the variable vector  $\mathbf{X}$ , it can be moved out of the expectation operation.

Based on Eq.(37), the obtained coefficients in environment  $e$ ,  $[\hat{\mathbf{W}}^e]_m^\top$ , is exactly the true causal coefficients  $[\mathbf{W}_0]_m^\top$ . Since  $m$  is any number in  $\{1, \dots, d\}$ , we have  $\hat{\mathbf{W}}^e = \mathbf{W}_0$ . The lemma is proved.  $\square$

To prove the Theorem 4.1, we further define two important terms - *stable graph* and *predecessor*.

**Definition C.3.** For a given graph  $G$ , if  $\exists \mathbf{S}, \mathbf{W}$  such that:

$$\mathcal{G}(\mathbf{S}) = \mathcal{G}(\mathbf{W}) = G \quad (38)$$

$$\mathbf{W} = \arg \min_{\overline{\mathbf{W}}} \mathcal{L}^e(\mathbf{S} \circ \overline{\mathbf{W}}), \quad \forall e \in \mathcal{E} \quad (39)$$

Then we say  $G$  is a stable graph.

**Definition C.4.** For two nodes  $X_1$  and  $X_2$  in a DAG, if  $X_2$  is reachable from  $X_1$ , then  $X_1$  is a predecessor of  $X_2$ . We denote all the predecessors of  $X_2$  in graph  $G_0$  as  $Pre_0(X_2)$ .

With Definition C.3, we further denote the parents of the variable  $X_i$  in  $G_0$  as  $Pa_0(X_i)$  and the corresponding indexes as  $Pa_0(i)$ . We propose the following Lemma C.5 to demonstrate that the causal directions between any two variables cannot violate each other in any stable graph and the true causal graph.

**Lemma C.5.** If  $G_s$  is a stable graph, and given the conditions in Theorem 4.1, then  $\forall X_i \in \mathcal{V}$  such that  $X_i$  is not the source node,  $\forall X_j \in Pa_s(X_i)$ , we have:  $X_i \notin Pre_0(X_j)$ .

*Proof.* To prove the lemma, we only need to show that given any  $X_i \in \{X_1, \dots, X_d\}$  without being the source node, if  $\exists X_j$  such that:

$$X_j \in Pa_s(X_i), \quad X_i \in Pre_0(X_j) \quad (40)$$

Then  $G_s$  cannot be a stable graph.

To achieve this, we need to incorporate the information of the environment  $e$ . Given  $j$  satisfying Eq.(40), we aim to find  $j_0$  such that:

$$X_{j_0} \in Pa_s(X_i), \quad z_{j_0} \perp Pa_s(X_i) \setminus X_{j_0} \quad (41)$$

Suppose there exists  $j$  satisfying Eq.(40), we will find  $j_0$  with the following process:

- (1) Set  $j_0$  to be  $j$ ;
- (2) If  $\exists X_k \in Pa_s(X_i)$  such that there exists the path from  $X_{j_0}$  to  $X_k$ , then we set  $j_0$  to be  $k$ . In this step, the condition  $X_i \in Pre_0(X_{j_0})$  still holds. If there is no such  $X_k \in Pa_s(X_i)$  satisfying the above condition, we will exit the iteration.

In this iteration, we always have  $X_i \in Pre_0(X_{j_0})$ . Also, with the above process, we know that  $\forall X_k \in Pa_s(X_i) \setminus \{X_{j_0}\}, X_{j_0} \notin Pre_0(X_k)$ , which means:

$$z_{j_0}^e \perp X_k \mid \forall k \in Pa_s(i) \setminus \{j_0\} \quad (42)$$

Now since the result of the regression from  $Pa_s(X_i)$  to  $X_i$  is exactly the  $m$ -th column of  $\hat{\mathbf{W}}^e$ , we denote the result of the regression based on Eq.(39) as:

$$\begin{aligned} [\hat{\mathbf{W}}^e]_m &= \arg \min_{[w_1, \dots, w_d]^\top} \mathbb{E}_e \| w_{j_0} X_{j_0} + \sum_{k \in Pa_s(m) \setminus \{j_0\}} w_k X_k - X_i \|_2^2 \\ &\text{s.t. } w_j = 0, \quad j \in \{1, \dots, d\} \setminus Pa_s(m) \end{aligned} \quad (43)$$

Then the optimal value for  $w_{j_0}$  is:

$$\hat{w}_{j_0}^e = \frac{\mathbb{E}_e[X_i X_{j_0}] - \sum_{k \in Pa_s(i) \setminus \{j_0\}} \hat{w}_k^e \mathbb{E}_e[X_k X_{j_0}]}{\mathbb{E}_e[X_{j_0}^2]} \quad (44)$$

According to the conditions of theorem 4.1, there exist two distinct environments  $e_1, e_2 \in \mathcal{E}$  such that  $Var(z_{j_0}^{e_1}) \neq Var(z_{j_0}^{e_2})$  and for any other node  $X_i$ , i.e.,  $i \neq j_0$ , we have  $Var(z_i^{e_1}) = Var(z_i^{e_2})$ .

Hence in the right term in Eq.(44), with  $X_i \perp z_{j_0}$  (according to the condition  $X_i \in Pre_0(X_{j_0})$ ), and  $\forall k \in Pa_s(X_i) \setminus \{j_0\}, z_{j_0}^e \perp X_k$  in Eq.(42), we could have:

$$\mathbb{E}_{e_1}[X_i X_{j_0}] = \mathbb{E}_{e_2}[X_i X_{j_0}]; \quad \forall k \in Pa_s(X_i) \setminus \{j_0\}, \mathbb{E}_{e_1}[X_k X_{j_0}] = \mathbb{E}_{e_1}[X_k X_{j_0}]; \quad (45)$$

If there exists  $k \in Pa_s(i) \setminus \{j_0\}$  such that  $\hat{w}_k^e$  is different across  $e_1$  and  $e_2$ , then  $G_s$  is already not stable, which raises the contradiction. Otherwise, if  $\hat{w}_k^{e_1} = \hat{w}_k^{e_2}, \forall k \in Pa_s(i) \setminus \{j_0\}$ , then since  $\mathbb{E}_{e_1}[X_{j_0}^2] \neq \mathbb{E}_{e_2}[X_{j_0}^2]$ , we will have  $\hat{w}_{j_0}^{e_1} \neq \hat{w}_{j_0}^{e_2}$ , indicating  $G_s$  is not a stable graph. The contradiction still exists.

Thus we can have the conclusion: If  $G_s$  is a stable graph, then  $\forall X_j \in Pa_s(X_i)$ , we have  $X_i \notin Pre_0(X_j)$ . The lemma is proved.  $\square$

With Definition C.3, we can rewrite Theorem 4.1 as:

**Theorem C.6.** For any stable graph  $G_s$ , we denote the corresponding structures for the true graph  $G_0$  and  $G_s$  as  $\mathbf{S}_0$  and  $\mathbf{S}_s$ , respectively. Also we denote the corresponding consistent optimal parameters as  $\mathbf{W}_0$  and  $\mathbf{W}_s$ . Then we have:

$$\sum_{e \in \mathcal{E}} \mathcal{L}^e(\mathbf{S}_0 \circ \mathbf{W}_0) \leq \sum_{e \in \mathcal{E}} \mathcal{L}^e(\mathbf{S}_s \circ \mathbf{W}_s) \quad (46)$$

The equation holds only for  $\mathbf{W}_0 = \mathbf{W}_s$ .

*Proof.* Note that in this case  $\mathbf{W}_0$  is the optimal parameters for  $G_0$ , and thus it is also the true coefficients for data generation. (as shown in Lemma C.2.)

To prove Theorem 4.1, we will split the regression loss in Eq.(31) to the specific loss value in every environment and every node except source nodes. In other words, we illustrate that for any environment  $e \in \mathcal{E}$ ,  $\mathcal{L}^e(\mathbf{S}_0 \circ \mathbf{W}_0) \leq \mathcal{L}^e(\mathbf{S}_s \circ \mathbf{W}_s)$ , which could directly lead to Eq.(46). Hence, in the following part, with a slight abuse of notation, we will omit the superscript  $e$ . We will show that  $\forall X_i \in \mathcal{V}$ , where  $\mathcal{V}$  is the node set, the regression loss from  $Pa(X_i)$  to  $X_i$  in  $G_s$  is larger or equal than in  $G_0$ , with the equaling condition holds when:

$$\text{i-th column}(\mathbf{W}_0) = \text{i-th column}(\mathbf{W}_s). \quad (47)$$

Given any  $X_i \in \mathcal{V}, i \in \{1, \dots, d\}$ , we denote all the parents of  $X_i$  in  $G_s, G_0$  as  $Pa_s(X_i), Pa_0(X_i)$  and the corresponding indexes of its parents as  $Pa_s(i), Pa_0(i)$ , respectively. Then the true generation process for the variable  $X_i$  could be denoted as:

$$X_i = \sum_{k \in Pa_0(i)} [\mathbf{W}_0]_{ki} X_k + z_i; \quad z_i \sim \mathcal{N}(0, \sigma_i^2) \quad (48)$$

When performing regression from  $Pa_s(X_i)$  to  $X_i$ , we need to constrain  $\mathcal{G}(\mathbf{W}_s) = G_s$ , which means

$$[\mathbf{W}_s]_{ki} = 0 \mid \forall k \in \{1, \dots, d\} \setminus Pa_s(i). \quad (49)$$

We denote the minimal loss and the optimal elements as

$$L_i^s = \min_{\{\bar{w}_k \mid k \in Pa_s(i)\}} \mathbb{E} \| X_i - \sum_{k \in Pa_s(i)} \bar{w}_k X_k \|_2^2 \quad (50)$$

$$\{w_k^* \mid k \in Pa_s(i)\} = \arg \min_{\{\bar{w}_k \mid k \in Pa_s(i)\}} \mathbb{E} \| X_i - \sum_{k \in Pa_s(i)} \bar{w}_k X_k \|_2^2 \quad (51)$$

where  $\{w_k^* \mid k \in Pa_s(i)\}$  is a set and its elements are exactly the corresponding elements of  $[\mathbf{W}_s]_i$ , i.e., the non-zero elements of  $i$ -th column of  $\mathbf{W}_s$ .

Then we define three sets of indexes as follows:

$$\mathcal{I}_u = Pa_0(i) \cap Pa_s(i); \quad \mathcal{I}_v = Pa_0(i) \setminus Pa_s(i); \quad \mathcal{I}_k = Pa_s(i) \setminus Pa_0(i)$$

Then after substituting Eq.(48) into Eq.(50), we have:

$$L_i^s = \min_{\{\bar{w}_k \mid k \in Pa_s(i)\}} \mathbb{E} \| \sum_{u \in \mathcal{I}_u} ([\mathbf{W}_0]_{ui} - \bar{w}_u) X_u + \sum_{v \in \mathcal{I}_v} [\mathbf{W}_0]_{vi} X_v + \sum_{k \in \mathcal{I}_k} \bar{w}_k X_k + z_i \|_2^2 \quad (52)$$

According to Lemma C.2,  $\forall X_j \in Pa_s(X_i)$ , we have  $X_i \notin Pre_0(X_j)$ , which means  $X_j \perp z_i$ . Thus we have  $z_i \perp Pa_s(X_i)$ . By definition, we have  $z_i \perp Pa_0(X_i)$ , which yield  $z_i \perp \{Pa_s(X_i) \cup Pa_0(X_i)\}$ . Then we can rewrite the above equation as:

$$L_i^s = \min_{\{\bar{w}_k \mid k \in Pa_s(i)\}} \mathbb{E} \| \sum_{u \in \mathcal{I}_u} ([\mathbf{W}_0]_{ui} - \bar{w}_u) X_u + \sum_{v \in \mathcal{I}_v} [\mathbf{W}_0]_{vi} X_v + \sum_{k \in \mathcal{I}_k} \bar{w}_k X_k \|_2^2 + \sigma_i^2 \quad (53)$$

Since the reconstruction loss for  $X_i$  in the true graph  $G_0$ , denoted as  $L_i^0$  is exactly the variance of the additive noise added on  $X_i$ , i.e.,  $\sigma_i^2$ . Thus here we already have  $L_i^s \geq L_i^0 = \sigma_i^2$ . In the following part, We will explore the conditions that make the equation hold exactly.

Note that  $\forall j \in Pa_0(i)$ , we have  $[\mathbf{W}_0]_{ji} \neq 0$ . Then for all the nodes in  $\mathcal{I}_u \cup \mathcal{I}_v \cup \mathcal{I}_k$ , there must exists a node denoted as  $X_{end} \in \mathcal{I}_u \cup \mathcal{I}_v \cup \mathcal{I}_k$  that has no successors in  $\mathcal{I}_u \cup \mathcal{I}_v \cup \mathcal{I}_k$  according to  $G_0$ . This means the noises corresponding to  $X_{end}$  will be independent from all the other nodes in  $\mathcal{I}_u \cup \mathcal{I}_v \cup \mathcal{I}_k$ . Then we discuss three situations for  $X_{end}$  to be in  $\mathcal{I}_u, \mathcal{I}_v$ , and  $\mathcal{I}_k$ , respectively:

- If  $X_{end} \in \mathcal{I}_u$ , we denote the index for  $X_{end}$  as  $u_1$ . Then we have:

$$\begin{aligned} L_i^s - L_i^0 &\geq \min_{\{\bar{w}_k | k \in Pa_s(i)\}} \mathbb{E} \left\| \sum_{u \in \mathcal{I}_u \setminus \{u_1\}} ([\mathbf{W}_0]_{ui} - \bar{w}_u) X_u \right. \\ &\quad \left. + \sum_{v \in \mathcal{I}_v} [\mathbf{W}_0]_{vi} X_v + \sum_{k \in \mathcal{I}_k} \bar{w}_k X_k \right\|_2^2 + ([\mathbf{W}_0]_{u_1 i} - \bar{w}_{u_1})^2 \sigma_{u_1}^2 \end{aligned}$$

Then the minimum operation  $\min_{\{\bar{w}_k | k \in Pa_s(i)\}}$  in Eq.(50) will directly set the optimal value of  $\bar{w}_{u_1}$ , i.e.,  $w_{u_1}^*$  to be  $[\mathbf{W}_0]_{u_1 i}$ .

- If  $X_{end} \in \mathcal{I}_v$ , we denote the index for  $X_{end}$  as  $v_1$ . Then we have:

$$\begin{aligned} L_i^s - L_i^0 &\geq \min_{\{\bar{w}_k | k \in Pa_s(i)\}} \mathbb{E} \left\| \sum_{u \in \mathcal{I}_u} ([\mathbf{W}_0]_{ui} - \bar{w}_u) X_u \right. \\ &\quad \left. + \sum_{v \in \mathcal{I}_v \setminus \{v_1\}} [\mathbf{W}_0]_{vi} X_v + \sum_{k \in \mathcal{I}_k} \bar{w}_k X_k \right\|_2^2 + [\mathbf{W}_0]_{v_1 i}^2 \sigma_{v_1}^2 \end{aligned}$$

In this case, we will have the strict inequality  $L_i^s > L_i^0$ , which means the reconstruction loss for  $G_s$  will be strictly larger than  $G_0$ .

- If  $X_{end} \in \mathcal{I}_k$ , we denote the index for  $X_{end}$  as  $k_1$ . Then we have:

$$\begin{aligned} L_i^s - L_i^0 &\geq \min_{\{\bar{w}_k | k \in Pa_s(i)\}} \mathbb{E} \left\| \sum_{u \in \mathcal{I}_u} ([\mathbf{W}_0]_{ui} - \bar{w}_u) X_u \right. \\ &\quad \left. + \sum_{v \in \mathcal{I}_v} [\mathbf{W}_0]_{vi} X_v + \sum_{k \in \mathcal{I}_k \setminus \{k_1\}} \bar{w}_k X_k \right\|_2^2 + \bar{w}_{k_1}^2 \sigma_{k_1}^2 \end{aligned}$$

Then the minimum operation  $\min_{\{\bar{w}_k | k \in Pa_s(i)\}}$  in Eq.(50) will directly set the optimal value of  $\bar{w}_{k_1}$ , i.e.,  $w_{k_1}^*$  to be 0.

If  $X_{end} \in \mathcal{I}_v$ , then we can already have  $L_i^s > L_i^0$ . For the other two situations, we will remove  $X_{end} \in \mathcal{I}_u$  or  $\mathcal{I}_k$  to form the new set  $\mathcal{I}'_u$  and  $\mathcal{I}'_k$ , then find the new  $X_{end}$  in  $\mathcal{I}'_u \cup \mathcal{I}_v \cup \mathcal{I}'_k$  to perform the above process again. According to this discussion, we could easily give the necessary and sufficient conditions for  $L_i^s$  to be equal to  $L_i^0$ :

- $\mathcal{I}_v = \emptyset$ . If not, then there must be one step of removing the current  $X_{end}$  such that  $X_{end} \in \mathcal{I}_v$ , which will directly lead to  $L_i^s > L_i^0$ .
- $\forall u \in \mathcal{I}_u, w_u^* = [\mathbf{W}_0]_{ui}$ .
- $\forall k \in \mathcal{I}_k, w_k^* = 0$ .

Now we have the optimal values:  $\{w_u | u \in \mathcal{I}_u\}$  and  $\{w_k | k \in \mathcal{I}_k\}$ . Besides, according to the definition of  $\mathcal{I}_u$  and  $\mathcal{I}_k$ , and  $\mathcal{I}_v = \emptyset$ , we have:  $\mathcal{I}_u \cup \mathcal{I}_k = Pa_s(j)$  and  $\mathcal{I}_u = Pa_0(i)$ . Since  $\mathcal{I}_k \cap Pa_0(i) = \emptyset$ , we have:  $\forall k \in \mathcal{I}_k, [\mathbf{W}_0]_{ki} = 0$ .

Since the structure of  $\mathbf{W}_s$  and  $\mathbf{W}_0$  need to be constrained to be the same as  $G_s$  and  $G_0$ , respectively, we must have:

$$[\mathbf{W}_0]_{ji} = [\mathbf{W}_s]_{ji} = 0, \quad \forall j \in \{1, \dots, d\} \setminus (\mathcal{I}_u \cup \mathcal{I}_k) \quad (54)$$

Then according to the above conditions, we have:

$$\text{i-th column}(\mathbf{W}_0) = \text{i-th column}(\mathbf{W}_s).$$

which is Eq.(47). Since  $X_i$  is any variable except source node in  $\mathcal{V}$ , we could have  $\mathbf{W}_0 = \mathbf{W}_s$ . (Note that for the columns corresponding to the source node, all the elements in these columns should be zero such that  $\mathcal{G}(\mathbf{W}_s) = G_s$  and  $\mathcal{G}(\mathbf{W}_0) = G_0$ ).

We conclude the proof of Theorem C.6. □

## D Additional Experimental Settings

### D.1 Dataset Generation

For the linear setting, after generating the graph, we randomly select  $\lfloor 0.3 * d \rfloor$  nodes in this graph, and then build  $\lfloor 0.3 * d \rfloor$  new nodes. We call these new variables as the environment variables and denote them as  $E$ , and they satisfy the same distributions and are all independent from each other. Then we create  $\lfloor 0.3 * d \rfloor$  edges from each environment node to the each selected node. In this way, we could simulate different environments with varying the distribution of the environment variables  $E$ . Then given this new graph with  $d + \lfloor 0.3 * d \rfloor$  nodes, we simulate random edge weights to obtain a new matrix  $\mathbf{W} \in \mathbb{R}^{(d + \lfloor 0.3 * d \rfloor) \times (d + \lfloor 0.3 * d \rfloor)}$ . With  $\mathbf{W}$ , we sample  $\mathbf{X} = \mathbf{W}^T \mathbf{X} + z \in \mathbb{R}^{d + \lfloor 0.3 * d \rfloor}$  with  $z$  from Gaussian noise model to generate 10 random datasets  $\mathbf{X}_e \in \mathbb{R}^{n \times (d + \lfloor 0.3 * d \rfloor)}$ . Then we remove the column corresponding to the additional  $\lfloor 0.3 * d \rfloor$  environment variables  $E$  to generate the final datasets  $\mathbf{X} \in \mathbb{R}^{n \times d}$ . We change the variances of the noises of the environment variables  $E$  to simulate different environments. In the nonlinear setting, after generating the graph, we randomly select  $\lfloor 0.5 * d \rfloor$  nodes in the graph, and then create  $\lfloor 0.5 * d \rfloor$  environment nodes and also  $\lfloor 0.5 * d \rfloor$  edges from each environment node to the selected node. Then given this new graph, we simulate the SEM  $\mathbf{X}_j = F_j(\mathbf{X}_{pa(j)}) + z_j$  for all  $j \in \{1, \dots, d + \lfloor 0.5 * d \rfloor\}$  in topological order. For the environment variables, we vary the distributions of the noises in different environments. Then for the other nodes, we set the distribution of the noises as  $\mathcal{N}(0, 1)$ . We choose  $f_j$  to be Additive Noise Models with two-layer MLPs. We will also remove the column corresponding to the variable  $E$  to generate the datasets  $\mathbf{X} \in \mathbb{R}^{n \times d}$ .

### D.2 Baselines

We select four state-of-the-art causal discovery methods for comparison:

- CD-NOD [16]. This is a constrained-based causal discovery method designed for heterogeneous datasets, *i.e.*, datasets from different environments. CD-NOD utilizes the independent changes across environments to determine the causal orientations, and proposes constrained-based and kernel-based methods to find the causal structure.
- NOTEARS [51]. This is specifically designed for linear setting, and is also the backbone of DICD in linear cases. NOTEARS estimates the true causal graph by minimizing the reconstruction loss with the continuous acyclicity constraint. We re-implement NOTEARS with replacing the L-BFGS-B iteration with Adam gradient descent, which could yield compatible performance and more importantly, could be deployed on GPU.
- NOTEARS-MLP [52]. This is specifically designed for nonlinear setting, which also serves as the foundation of DICD in nonlinear situations. NOTEARS-MLP approximates the generative SEM model by MLP while only constraining the first layer of the MLP with the continuous acyclicity constraint.
- DAGGNN[47]. DAGGNN formulates causal discovery with variational autoencoder, where the encoder and decoder are all graph neural networks. Choosing the evidence lower bound as the loss function and slightly modifying the acyclicity constraint, DAGGNN could manage to recover the weighted adjacency matrix.
- NoCurl [48]. NoCurl utilizes a two-step procedure: first find an initial cyclic solution, then employ Hodge decomposition of graphs and learn an acyclic graph by projecting the cyclic graph to the gradient of a potential function.
- DARING [13]. DARING imposes explicit residual independence constraint with an adversarial strategy. We choose the backbone as NOTEARS-MLP to conform with the settings above.

### D.3 Hyperparameter settings

For linear settings, there are two hyper-parameters in total:  $\lambda_1$  for the  $l_1$ -norm regularization term;  $\lambda_D$  for the DICD penalty term. We tune  $\lambda_1$  in  $\{0.01, 0.1\}$  for NOTEARS and DICD. Besides, we tune  $\lambda_D$  in  $\{0.1, 1\}$  for DICD. Then for nonlinear settings, there are three hyper-parameters in total:  $\lambda_1, \lambda_2, \lambda_D$ , among which  $\lambda_1$  and  $\lambda_2$  are for the  $l_1$ -norm and  $l_2$ -norm regularization terms, respectively.

We tune  $\lambda_1, \lambda_2$  both in  $\{0.01, 0.1\}$  and  $\lambda_D$  in  $\{0.1, 1\}$ . The scheduler for  $\lambda$  in Eq.(14) and Eq.(17) is shown as follows:

$$\lambda = \begin{cases} \frac{k}{K/3} \circ \lambda_D & k \leq K/3 \\ \lambda_D & K/3 \leq k \leq 2K/3 \\ \frac{K-k}{K/3} \circ \lambda_D & k \geq 2K/3 \end{cases} \quad (55)$$

where  $K$  is the estimated total step, and  $k$  is the current iteration. The intuition behind this scheduler is that we need to let the model fit the data at the beginning, then as the training process goes, we need to enforce our penalty to help find the true causal graph. Then for the last stage, the graph structure has almost been inferred. We need to gradually remove our penalty to let the structural causal function with the given structure fit the data.

#### D.4 Evaluation Protocols

We use the three most popular metrics in causal discover: false discovery rate(FDR), true positive rate(TPR) and structural Hamming distance(SHD). Higher TPR stand for better performances, while FDR and SHD should be lower to represent the better strategies.

#### D.5 Dataset Details

We provide the details of the dataset in this section. The details for the synthetic dataset have already been illustrated in Section 5.1.1. We need to provide more details for the dataset MNIST. We sample 10000 images in total, and 2000 images for each environment. We classify MNIST digits from 2 classes, where classes 0 and 1 indicate original digits (0,1,2,3,4) and (5,6,7,8,9). Then for each environment, we select the ratio of class 0 being green, which is shown in the "Ratio" column in Table 6. Then the noise variances(i.e. noise scale) for each environment are provided in the "Noise Scale" column in Table 6.

Table 6: Experimental Settings for Colored MNIST.

Environment	Ratio	Noise Scale
$e_1$	0.16	10/255
$e_2$	0.32	20/255
$e_3$	0.48	30/255
$e_4$	0.64	40/255
$e_5$	0.80	50/255

## E Additional Experiments

### E.1 Main Results

We provide the experimental results with the node number as  $d = 100$  and edge number  $s_0 = 400$ . The results in linear setting is provided in Table 7, and the results for nonlinear setting are in Table 8.

#### E.1.1 The effect of the imbalance between different environments

Since the imbalance of data is the major problem in machine learning, we aim to explore how the imbalance of data size between different environments would affect the performances of our method and other baselines. The total number of samples in this dataset is 1000 for linear settings and 2000 for nonlinear settings. We choose ER graphs with  $d = 20$  and  $s_0 = 4d = 80$  for this case study. The noises for the variable  $E$  in two environments are set to be  $\{0.2, 0.4\}$ . Then the ratio

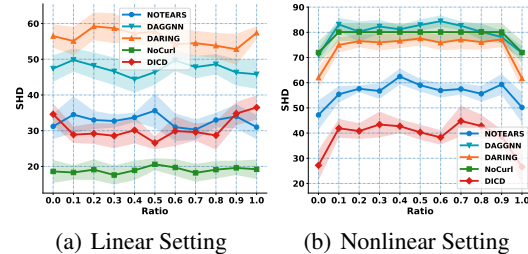


Figure 4: SHD for different percentage of imbalance between two environments in linear and nonlinear settings.

Table 7: Linear Setting, for ER and SF graphs of 100 nodes

Method	ER4			SF4		
	FDR	TPR	SHD	FDR	TPR	SHD
NOTEARS	<b>0.17±0.03</b>	0.78±0.03	147.9±15.7	<b>0.12±0.04</b>	0.91±0.02	81.4±23.0
DAGGNN	0.23±0.03	0.79±0.04	178.3±9.6	0.31±0.02	0.92±0.01	195.3±20.4
NoCurl	0.25±0.01	<b>0.94±0.00</b>	136.0±5.3	0.14±0.04	<b>0.98±0.01</b>	69.8±23.2
DARING	0.29±0.02	0.69±0.04	234.0±14.3	0.29±0.01	0.90±0.01	180.9±5.4
DICD	0.20±0.03	0.87±0.01	<b>133.9±16.2</b>	0.12±0.03	0.97±0.01	<b>61.9±15.6</b>

Table 8: Nonlinear Setting, for ER and SF graphs of 100 nodes

Method	ER4			SF4		
	FDR	TPR	SHD	FDR	TPR	SHD
NOTEARS	0.20±0.04	0.40±0.07	270.0±24.1	<b>0.17±0.06</b>	0.42±0.10	260.1±27.3
DAGGNN	0.52±0.05	0.09±0.01	390.6±7.7	0.50±0.08	0.09±0.02	390.3±13.4
DARING	0.41±0.05	0.15±0.02	367.0±8.8	0.42±0.04	0.15±0.02	367.3±6.9
NoCurl	0.62±0.06	0.23±0.02	447.2±33.0	0.60±0.03	0.18±0.02	418.6±10.7
DICD	<b>0.18±0.05</b>	<b>0.54±0.10</b>	<b>226.6±23.1</b>	0.18±0.03	<b>0.53±0.06</b>	<b>228.0±16.3</b>

in Figure 4 means the percentage of the samples from the first environment. From this figure, we could have the following observations: (1) In most of the settings, DICD outperforms other methods consistently, except when the data is higher imbalanced in linear setting, where there is almost only one environment. (2) In both linear and nonlinear settings, the balanced situation is the best for DICD, which means we have enough information from every environment. (3) Even there is only one group, DICD could make significant improvements against NOTEARS, which coincides with the discovery in Section 5.3.1.

### E.1.2 Running time Comparison between CD-NOD and DICD

We only record the running time of CD-NOD in nonlinear settings, since its running time is almost unacceptable in these cases. Then we report the averaged running time for different seeds and different graph types (ER or SF). From the table, we can observe that CD-NOD is very expensive for nonlinear cases, while the running time of DICD almost remain constant when the number of nodes get larger.

Table 9: Running time comparison

	10 nodes	20 nodes	50 nodes
CD-NOD	>9h	>64h	>300h
DICD	15min	15min	15min